Mathematical and optimization modelling in desalination: State-of-the-art and future direction

Farah Ejaz Ahmed[1], Raed Hashaikeh[1], Ali Diabat[2,3], Nidal Hilal[1,4,*]

[1] NYUAD Water Research Center, New York University Abu Dhabi, Abu Dhabi, United Arab Emirates

[2] Division of Engineering, New York University Abu Dhabi, Saadiyat Island, 129188, Abu Dhabi, United Arab Emirates

[3] Department of Civil and Urban Engineering, Tandon School of Engineering, New York University, Brooklyn, NY 11201, United States of America

[4] Centre for Water Advanced Technologies and Environmental Research (CWATER), College of Engineering, Swansea University, Fabian Way, Swansea SA1 8EN, UK

* Corresponding author, Email: n.hilal@swansea.ac.uk

Abstract

The growing water demand across the world necessitates the need for new and improved processes as well as for a better understanding of existing processes. This level of understanding includes predicting system performance in scenarios that cannot always be evaluated experimentally. Mathematical modelling is a crucial component of designing new and improved engineering processes. Through mathematically modelling real life systems, we gain a deeper understanding of processes while being able to predict performance more effectively. Advances in computational capacity and the ease of assessing systems allow researchers to study the feasibility of various systems. Mathematical modelling studies enable optimization performance parameters while minimizing energy requirements and, as such, have been an active area of research in desalination. In this review, the most recent developments in mathematical and optimization modelling in desalination are discussed with respect to transport phenomena, energy consumption, fouling predictions, and the integration of multiple scaling evolution on heat transfer surfaces has been reviewed. Similarly, developments in optimization of novel reverse osmosis (RO) configurations have been analyzed from an energy consumption perspective. Transport models for membrane-based desalination processes, including relatively less understood processes such as nanofiltration and forward osmosis are presented, with recent modifications to allow for different solutes and solutions. Mathematical modelling of hybrid systems integrated with RO has also been reviewed. A survey of the literature shows that mathematical and optimization modelling of desalination processes is an exciting area for researchers in which future scholarship includes coupling of renewable energy systems with desalination technologies, as well as more advanced descriptions of fouling evolution other than that of cake filtration in membrane-based processes.

Keywords: modelling, optimization, desalination, reverse osmosis, water treatment

Contents

1. Introduction

Between 2015 and 2050, the world population is projected to increase by 35% causing an even more rapid increase in the demand for water [1]. Despite being an abundant resource, fresh water needed for human consumption makes up a tiny fraction of the water on earth [2]. In addition, the amount of fresh water stays constant while our water demands are on the rise [3]. Millions of people die annually due to the lack of adequate water supply and proper sanitation. Many solutions have been proposed to help meet growing water demands, including better water resource management, increased water reuse and desalination. Many of the world's communities affected by drought have access to brackish ground water and seawater that can be converted to fresh water through desalination to help meet their water demands [2]. Consequently, the global demand for desalination is increasing [4], as is evident by the rapid desalination market growth in recent years. Globally, desalination plants produce around 95 million m^3/day. The Middle East and North Africa (MENA) regions are responsible for 48% of the global installed desalination capacity [5, 6].

1.1 Overview of desalination technologies

Desalination technologies are typically classified as either thermal or membrane-based technologies. Although membrane technology, specifically reverse osmosis (RO), makes up the majority of installed desalination capacity worldwide, thermal desalination remains the dominant technology in the Middle East. The two major thermal desalination technologies employed are multi-evaporation distillation (MED) and multistage flash (MSF), both of which are in an advanced growth phase, likely to reach saturation before 2050, as identified by Mayor [7]. On the other hand, most of the newly installed desalination capacity around the world operates on RO

membranes, which not only are more energy efficient than thermal desalination processes, but also provide modularity and ease of operation [7].

1.1.1. Thermal desalination

Although surpassed by reverse osmosis in terms of global installed capacity, thermal desalination plants are still dominant in the Middle East, where they are often integrated with power plants and are known to have long lifetimes of up to 30 years [8, 9]. Thermal desalination technologies such as MED and MSF rely on the principle of evaporation, which is the creation of a hot surface with heating steam, which then condenses on one side of the surface, allowing vapor to form on the other side [10]. Evaporator surfaces are of many types: submerged tube, falling films and plates, etc. [11]. Applications and limitations of each of these are discussed thoroughly in [12].

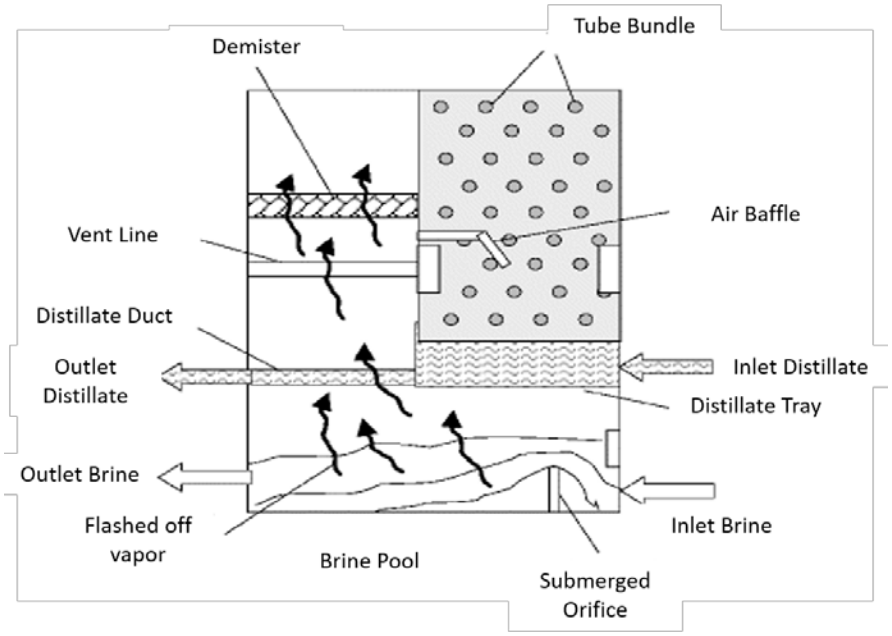

Figure 1: Schematic of flashing stage in MSF [12]

Separation in MSF occurs when some of the feed is evaporated in consequent stages by flashing. Figure 1 shows a schematic of a single flashing stage in MSF. The hot feed water is met with a lower pressure than its vapor pressure in each subsequent stage, causing some of the feed to flash.

The vapor formed in each stage passes through a demister and condenses on the external surface of the tube bundle [12]. The simplest design, known as once-through MSF (OT-MSF), involves returning the brine leaving the last stage back to the sea as brine blow down. The brine leaving the last stage of the MSF can be returned to the sea as brine blow down, a configuration known as once through MSF (MSF-OT). Another configuration which is known as brine mixing MSF (BM-MSF) involves mixing a portion of the brine from the last stage with the incoming feed.

In each subsequent stage, the temperature is reduced by flashing, boiling point elevation and non-equilibrium losses. The highest temperature at the inlet of the first stage is known as top brine temperature (TBT), while the difference between the TBT and the brine temperature in the final stage is known as the overall temperature difference [13].

Modelling an MSF system requires formulation of material balance, energy balance and momentum balances, such that the model predicts output stream variables for each stage, given input stream variables and stage parameters, as shown in Figure 2.

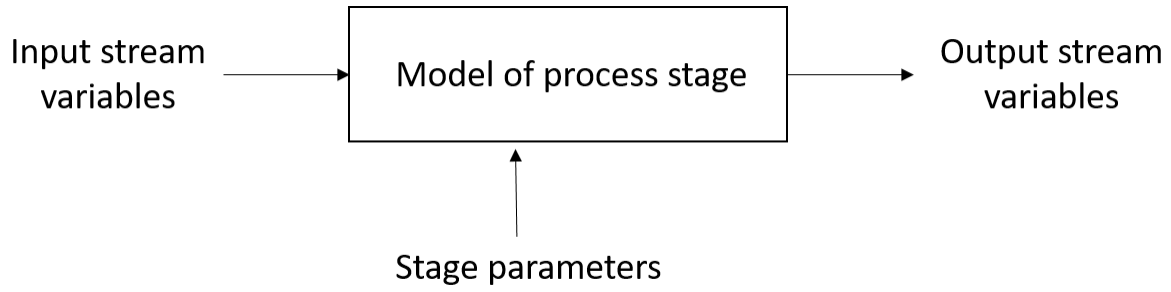

Figure 2: Depiction of a process model as a set of relationships between the input and output streams for an MSF stage [14]

The independent variables for each stream include the mass flow rate, temperature, salt concentration and pressure. Material balance and energy balance for thermal systems have been used to understand the transport phenomena in thermal desalination over a period of several decades [14-16], and thus are not reviewed here.

1.1.2 Membrane-based desalination

Various membrane-based separation processes exist, each one distinct in the size of particles or solutes it can retain, as shown in Figure 3. Only nanofiltration (NF) and RO are used for removing dissolved ions from aqueous streams, while others, such as ultrafiltration and microfiltration, are often used as pretreatment to RO as they remove larger particles. The most widely employed membrane-based desalination technology is RO, as mentioned above. The membrane material and structure play a critical role in transport properties and hence in membrane performance [17]. Membrane technology has the advantage of being modular, and attention to new configurations of the membrane module as well as the flow streams have enabled reduction in energy consumption.

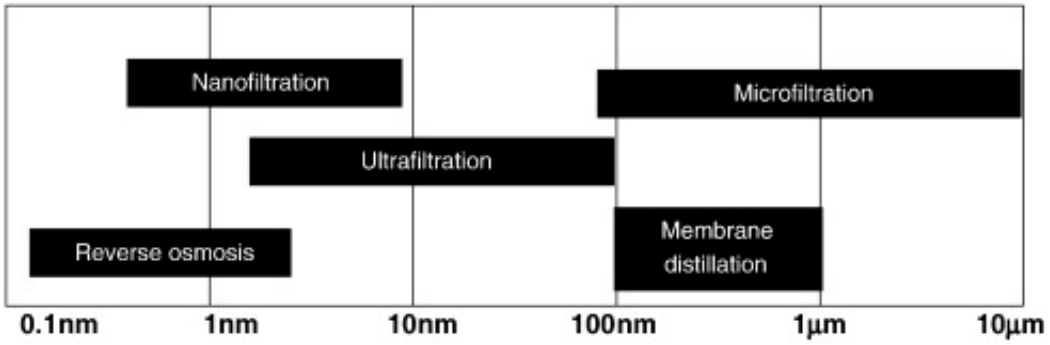

Figure 3: Spectrum of membrane separation processes [17]

1.1.2.1 Reverse osmosis

More than 60% of the world's installed desalination capacity operate with reverse osmosis (RO). RO is a pressure-driven process in which a dense semipermeable membrane allows the selective passage of water molecules through the membrane. In reverse osmosis, the phenomenon of natural osmosis, in which the solvent will flow from the region of low solute concentration to high solute concentration, is reversed by application of a hydraulic pressure greater than the difference in osmotic pressures between the feed side and permeate side, forcing the solvent to move from the

region of high salt concentration to low salt concentration (Figure 4) [18].

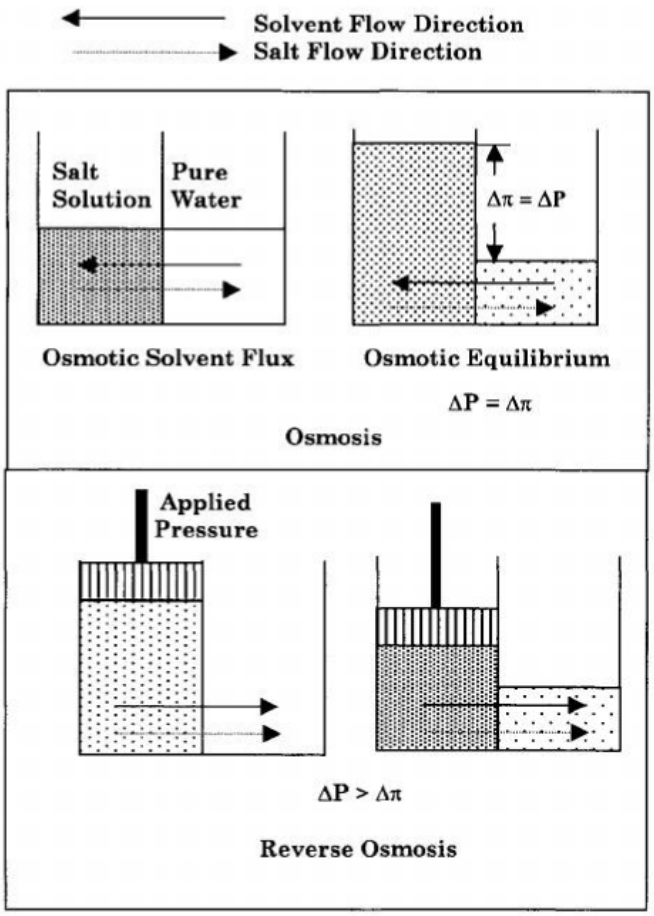

Figure 4: Osmosis and reverse osmosis processes [19]

In osmosis, water spontaneously passes from the low-salt concentration side to the high-salt concentration side until an osmotic equilibrium is reached between both sides. However if a pressure greater than the osmotic pressure is applied as is the case in reverse osmosis, the flow of water molecules is reversed and water will pass through the membrane from the high-salt concentration side to low-salt concentration side [20] Thus the effective pressure that drives water through the membrane is the difference between the applied pressure and the osmotic pressure. For simple systems, the osmotic pressure is calculated using the van't Hoff's equation described below:

$$\Delta\pi = v_i c_i \frac{RT}{MW}$$

where v_i is the number of ions in the dissociated salt, c_i is the concentration of salt in g/L, MW is the molar mass of the ion. As the expression for osmotic pressure contains molecular weight in the denominator, it can be seen that the osmotic pressure only comes into play for retention of very small solutes as is the case in RO and NF, but not for UF or MF.

Although many models have been developed for transport across RO membranes, the solution diffusion model for non-porous membranes remains the most widely accepted. It assumes that both solvent and solute dissolve in and diffuse across the membrane down a concentration gradient and this diffusion depends on the chemical potential of each, which is a function of the concentration and pressure gradients across the membrane (Figure 5) [21]. In other words, Brownian diffusion, flush and jump diffusion allow water to permeate through the membrane. The interactions of water and ions with the membrane depend strongly on the membrane structure [22, 23].

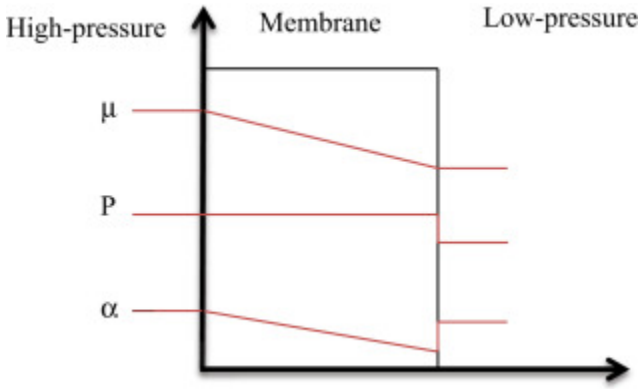

Figure 5: Assumptions of solution-diffusion model showing chemical potential (μ), pressure (P), and activity gradients across membrane (a).

The chemical potential difference in RO is given by:

$$\Delta\mu_i = RTln\,\Delta a_i + V_i\Delta P$$

where α_i is the activity of species i (solute or solvent), V_i is the molar volume, and Δp is the

pressure differential across the membrane [21]. RO is used to remove dissolved substances, including single charged ions from the aqueous feed streams [24]. Transport mechanisms for RO membranes are further discussed in detail in Section 2.2.1.

Reverse osmosis was first commercialized by Loeb and Sourirajan [25], who developed the first cellulose acetate membranes for RO. Ever since, RO has gained much commercial success and is currently the dominant desalination technology. New membrane materials, improved pretreatment methods and novel process design have enabled the technology to operate close to theoretical energetic limit. Innovations in system configuration such as the use of multiple stages and/or passes have been incorporated in largescale RO plants [26], mainly to overcome drawbacks of the single-stage RO process in which the large applied pressure results in avoidable energy dissipation and high initial permeate flux. Current developments focus on configuration improvements as well as hybridization of RO with other technologies with the aim of further reducing energy costs.

1.1.2.2 Nanofiltration

On the separation spectrum, nanofiltration falls between ultrafiltration and reverse osmosis, and is thus a unique filtration process in which large salts and low molecular weight cut-off (MWCO) solutes can be separated from the feed stream. Also known as ‘loose RO’ membranes, NF membranes can be used to reduce salinity and are often used as pretreatment to other desalination processes such as RO, MSF, and MED. Ionic transport in NF membranes is still not fully understood and predicting NF performance usually requires structural and electrical characterization of the membrane. Due to its complexity, modelling of transport through NF is a topic of great interest among researchers. What is known is that ionic transport through NF membranes depends on charge, steric and dielectric effects [27, 28]. The first of these is a consequence of the charge polarities between the membrane and solutes, while the second effect

is due to the size of ions relative to membrane pores, while the third results from differences in dielectric constant between bulk and membrane pores [27]. Transport of solutes through NF is most widely modelled using the extended Nernst Plank (ENP) differential equations, which describe solute transport as a combination of diffusion, convection and electro-migration[21]. The evolution of these models to better predict NF performance to account for different solutions as well as developments in characterization of NF membranes are emphasized in Section 2.2.2. Rejection of divalent ions by NF is typically in the range of 75-99%, whereas monovalent ions are only rejected at 30-50% by NF membranes [29]. NF is used in several industries for various applications, as shown in Table 1.

Table 1: Commercial applications of NF membranes for aqueous and nonaqueous processes [30]

Industry	**Application**	**Solvent medium**
Water treatment	Water softening, color removal, micropollutants elimination, pretreatment to RO	Aqueous
Wastewater treatment	Leachate wastewater, textile effluent, emerging contaminants removal, effluent from pulp and paper process	Aqueous
Food and dairy	Whey pre-concentration, whey protein desalination, caustic and acid recovery, gelation concentration	Aqueous and nonaqueous
Pharmaceutical and biomedical	Fractionation of proteins, plasma purification, filtration of DNA, RNA and endotoxins, preparation of	Aqueous and nonaqueous

	desalted and concentrated antibiotics	
Oil and gas	Solvent recovery from lube oil and hydrocarbon solvent mixtures, removal of sulfate from seawater before offshore reservoir rejection	Aqueous and nonaqueous

1.1.2.3 Forward osmosis

Forward osmosis, as the name suggests, refers to the movement of molecules across a semipermeable membrane due to difference in osmotic pressure. This osmotic pressure difference is brought about using a concentrated draw solution on the permeate side, that 'draws' the water from the feed [31]. Due to this transport of water molecules across the membrane, the feed solution becomes more concentrated while the draw solution is diluted. As FO is an osmotically driven process that does not need external hydraulic pressure (as is the case for NF and RO), the energy requirements can be significantly lower than in RO. Transport of water in FO results from a water chemical potential gradient driven by a difference in the solute concentration on either side of the membrane [32]. This difference in solute concentration causes an osmotic pressure differential across the membrane, which results in a more concentrated feed stream and a more dilute permeate stream due to the transport of water through the membrane.

Membrane materials and choice of draw solution have been an active area of research in FO. Desalination using FO is a two-stage process, as shown in Figure 6: (1) FO which results in water permeating from feed to draw solution, and (2) regeneration of the dilute draw solution to recover pure water.

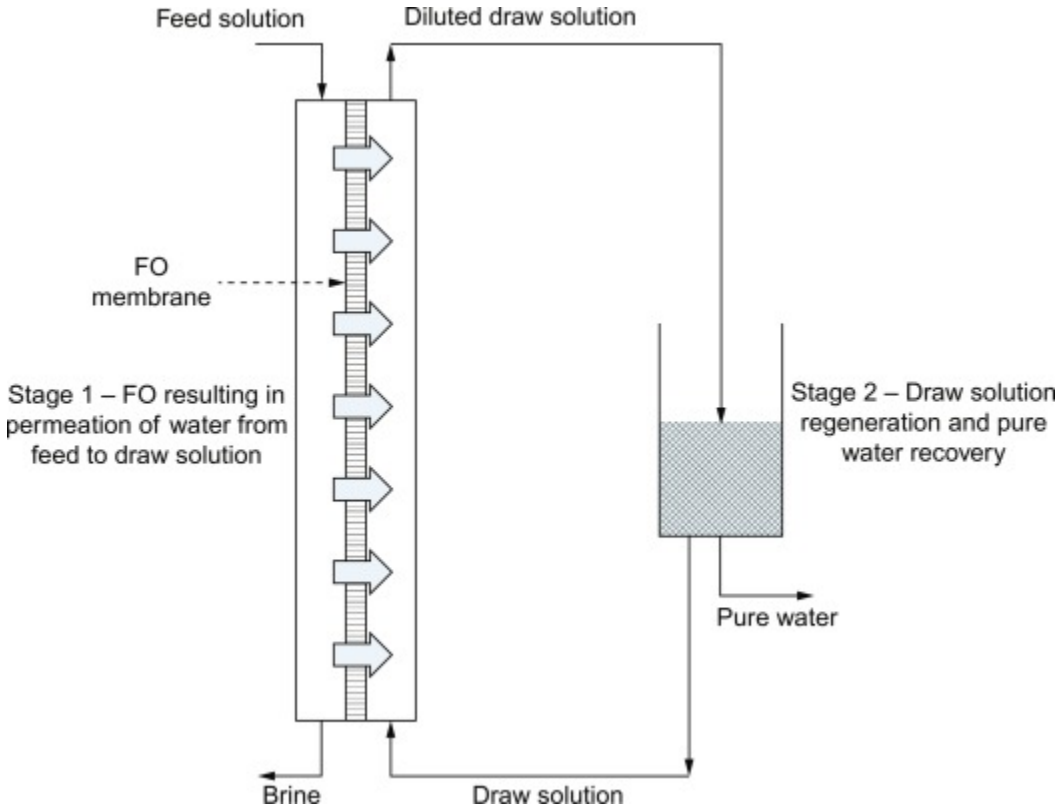

Figure 6: Schematic of the two stages of fresh water production with FO [33]

1.1.2.4 Fouling in membrane-based desalination

Membrane fouling is the accumulation of undesired substances either on the surface of the membrane, or inside its pores. As it reduces the effective surface area for desalination, fouling leads to undesirable consequences such as decrease in membrane flux (or increase in hydraulic pressure to maintain the same flux) and reduction in salt rejection [23]. Fouling mechanisms in high-pressure membrane processes differ from those in MF and UF in that surface fouling is the predominant fouling mechanism on the more compact and non-porous RO and NF membranes [34]. As fouling depends strongly on the physical and chemical interactions between foulants and membrane surface, the extent of fouling, or degree of attachment, is a function of feed composition, membrane properties, hydrodynamic conditions, cleaning strength and frequency. Fouling can be classified as colloidal, inorganic, organic and biofouling [35]. Fouling can also be aggravated by

the phenomenon of concentration polarization (CP). CP refers to the increase in salt concentration at the membrane surface as compared to the bulk salt concentration on the feed side of the membrane. It results from rejection of salt ions at the membrane surface as water passes through. Consequence of concentration polarization include: higher osmotic pressure at the membrane surface, increased salt passage through the membrane, increased potential of salt precipitation i.e. scaling at the membrane surface and increased fouling [36]. External CP described above has been extensively modelled in literature. Internal concentration polarization (ICP) is a related phenomenon that occurs only in osmotically driven processes such as FO. ICP is a reduction in osmotic pressure gradient across the active layer resulting from a sharp concentration gradient formed within the support layer of the membrane [37, 38]. It results in a sharp concentration gradient formed within the porous support layer.

1.2 Modelling in desalination

1.2.1 Why do we need mathematical and optimization modelling?

Mathematical modelling is the process of describing real world problems as mathematical equations and using some approaches to solve the mathematical equations as a guide to deconstructing and solving the original problem [39]. One of the most commonly applied types of mathematical modelling is optimization modelling or mathematical programming. An optimization model consists of maximizing or minimizing an objective function by systematically choosing input values from within a set that stratifies some constraints and computing the value of the function. Although real world problems cannot always be explained entirely by mathematical equations, mathematical solutions alone are also not practical as they take into account several simplifying assumptions. Optimization is the process of finding the best possible solution to a given problem by examining several alternatives [40]. In recent years, multiscale modelling and

optimization has gained significant interest with potential for better prediction and understanding of systems in material science, fluid mechanics, biology, chemistry, and physics [41].

With an unprecedented rise in computational capabilities, matched by an increase in the complexity of systems, mathematical modelling and optimization are now considered essential components of the design process. Today, we have access to powerful software tools that enable geometric modelling, meshing and visualization of results, as well as advanced computational algorithms [42]. In engineering, a model can be defined as an 'abstraction of reality', wherein a real world system can be understood more sufficiently and predictions can be made through analysis of an idealized form [43]. In engineering, mathematical and optimization modelling enables manipulation of design parameters to meet certain objectives and/or helps predict system performance. Engineering modelling is related to understanding an entire system and identifying key components under focus [43]. For any multifaceted process, accurate models with realistic assumptions that are not too complicated to solve are a challenge. The presence of uncertainties in real-life systems as well as the high costs associated with building pilot plants render the modelling approach all the more valuable, but also more complex with several constraints that need to be satisfied and development of models that match the real-world system as closely as possible [44]. Modelling enables better prediction and control of system performance and helps our understanding of everyday processes. However, developing suitable models requires a certain level of understanding of the mechanism(s) being studied. It can be argued that the modelling approach strongly complements experimental research and forms a critical component of research in any field.

1.2.2 Modelling approaches in desalination

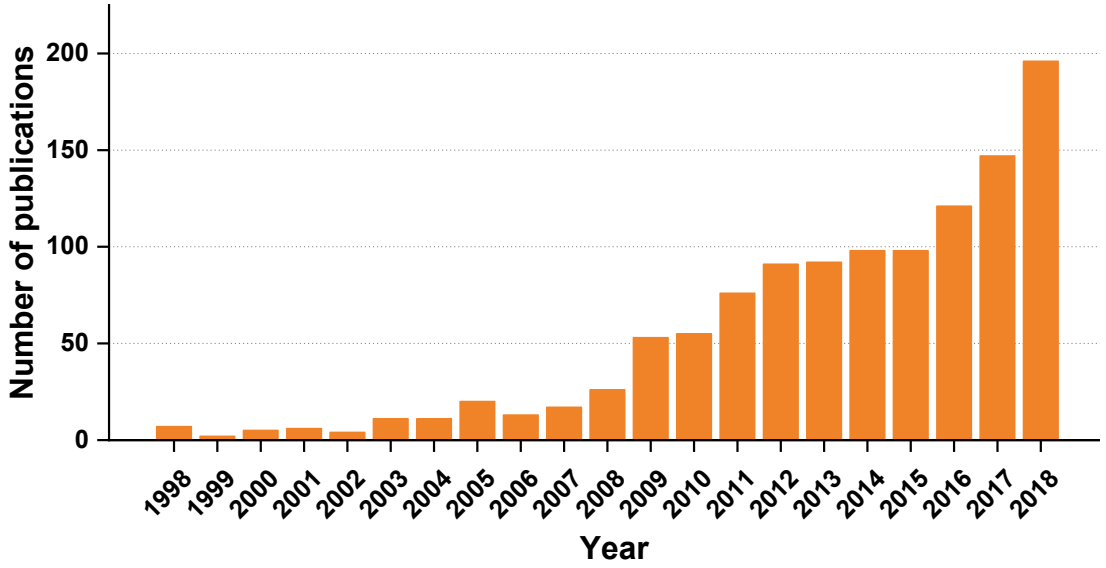

Figure 7: Publications with topic keywords: optimization modelling , desalination from 1998 to 2018 (Web of Science)

Interest in optimization modelling techniques in desalination has increased dramatically in the last decade, as shown in Figure 7. Van der Bruggen cites three critical benefits of process modelling specifically in pressure-driven membrane separation [45]. First, models help predict expected performance which, in turn, allows different membranes to be compared. Second, modelling provides a deeper understanding of the mechanisms responsible for permeation and separation, which is of particular value in newer, less understood processes. Finally, modelling allows for process monitoring and a study of the factors that affect performance characteristics for each process, helping us find configurations. The type of material and structure will determine the kind of mass transport through the membrane (solution, diffusion, Knudsen diffusion, convection, etc.) and, therefore, the mathematical model to be applied to describe the mass transfer (solution-diffusion model, pore-flow model, etc.). Modelling and control of RO desalination systems was previously reviewed by Sobana and Panda in 2011 [46]. Blanco-Marigorta reviewed differing approaches in literature for formulating exergetic efficiency of RO desalination plants [47]. A comprehensive review which includes recent developments in RO process optimization is missing

in literature. Although there have been reviews on developments of newer technologies such as forward osmosis (FO), modelling techniques in FO have not been discussed on their own [48].

In 2007, Weijuan et al. reviewed modelling techniques in nanofiltration membranes [49]. Later, Oatley-Radcliffe et al. highlighted the need for a reevaluation of NF modelling, especially for complex feeds in their review of existing modelling strategies [50]. Recently, Yaroshchuk et al. reviewed existing models for NF of electrolyte solutions in which they derive equations for ion transfer from linear irreversible thermodynamics and identify membrane properties that control membrane performance for NF of multi-ion solutions [51]. They also included the development of an advanced engineering model for NF of multi-ion solutions which relies on a solution diffusion electromigration mechanism. Interestingly, in another review on NF research trends, Oakley-Radcliffe et al. [52] linked a decline in the topic of nanofiltration modelling between 2009 and 2016 to limited practical understanding of the process, owing to the lack of drastic advances in measurement technologies of nanofiltration membranes and processes. The uncertainty of separation mechanisms stems from a lack of in-depth knowledge of the physical and electrical properties of real NF membranes [50]. However, although research in nanofiltration modelling was indeed stagnant or moving towards decline during this period, the last three years have shown a resurgence of interest in this area with more than a two-fold increase in the number of publications with ‘nanofiltration’ and ‘modelling’ in their title (Figure 8).

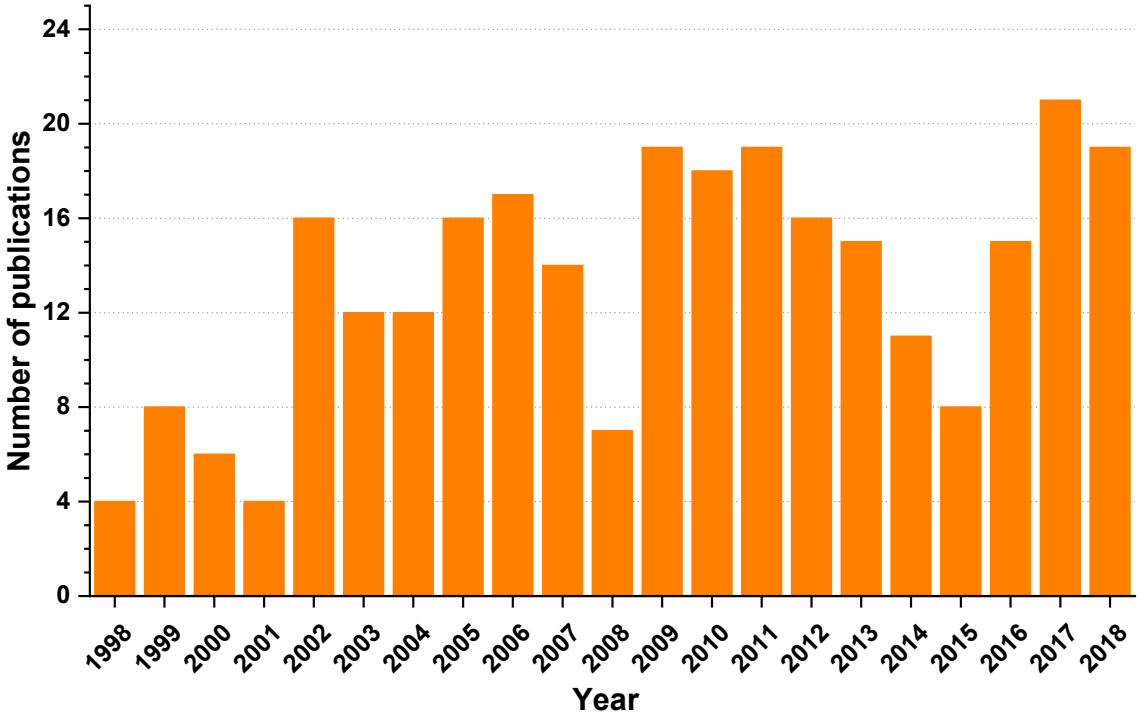

Figure 8: Number of publications with 'nanofiltration' and 'modelling' in title from 1998 to 2018 (Web of Science)

Apart from traditional mathematical modelling of processes, artificial intelligence (AI) techniques such as artificial neural network (ANN) are gaining attention in desalination, although the advent of AI in desalination has recently been reviewed by two different groups in the last year [53, 54]. As such, these have been left out of this review. In this review, developments of the last five years in modelling and optimization in desalination have been critically reviewed with respect to transport phenomena, energy consumption, fouling prediction and integration of multiple desalination technologies. This includes modelling of performance in more mature technologies such as MSF and RO from an energy consumption perspective. For relatively less understood processes such as NF and FO, simple transport models have been described, with a review of recent modifications to allow for different types and concentrations of solutes. Gaps in literature are identified, paving the way for future areas of research in modelling approaches to desalination.

2. Optimization modelling in desalination

2.1 Optimization modelling in Multistage Flash

2.1.1 Scale control in Multistage Flash (MSF)

Thermal desalination processes such as MSF and MED are mature technologies, whose lower competitiveness and energy efficiency in comparison to RO have limited the market to the Middle East, where the cost of energy is relatively low and the feed seawater is of higher, often aggressive, salinity [7, 55]. Fouling, which is the unwanted accumulation of solid materials on the heat transfer surface, increases the thermal resistance and leads to performance deterioration [56]. Scale formation or precipitation of certain salts on the heat transfer surfaces impedes the rate of heat transfer and reduces the efficiency of the heat transfer process, thus leading to increased specific energy consumption as well as the need for frequent cleaning. Scale formation can also lead to clogging and corrosion of heat exchangers and evaporators. Many recent modelling studies in thermal desalination focus on better understanding the formation of scale on heat transfer surfaces as well as modelling scale control strategies, both of which are highlighted in this review.

Various models have been developed to correlate the formation of scale on heat transfer surfaces over the last sixty years, and these models are not limited to desalination units. The earliest of these, proposed by Kern and Seaten, was based on a diffusion model in which the net rate of deposition is the difference between the rate of deposition and rate of removal at any given time, correlating an increase in fluid velocity with a reduction in fouling layer thickness [57, 58]. Over the years, further modifications were incorporated into ionic diffusion models as well as kinetic models to predict the rate of scale deposition as a function of operating parameters and the use of antiscalants, including the use of computational fluid dynamics (CFD) [59-65]. For a more comprehensive insight into the description of fouling of heat exchanger surfaces, including fouling

mechanisms, related mathematical modelling, and control of fouling, the reader is guided to other literature [66, 67]. This section will focus exclusively on developments between 2014 and 2019 in the modelling and optimization of fouling in MSF and MED systems. The presence of a series of connected heat exchangers in these systems means that the fouling behavior is often complex. Only recently have models been developed to account for the changing temperature and feed salinity from one stage to another, as well as variation of the fouling factors over time [68].

Scaling in thermal desalination processes is most commonly caused by precipitation of alkaline scales such as calcium carbonate ($CaCO_3$) and magnesium hydroxide ($Mg(OH)_2$) [69-72]. The rate of scale formation in seawater is a function of temperature, pH, concentration of bicarbonate ions, rate of CO_2 release, concentration of Ca^{2+} and Mg^{2+} ions, and total dissolved solids (TDS) [69, 73]. The rate of fouling is defined as the average deposit surface loading per unit surface area in a unit of time. Often, the thickness of the deposited layer and porosity are used to describe the extent of fouling on a heat exchange surface [67]. Effective scale control requires accurate calculations of the amount of scale formation [74]. Alsadaie and Mujtaba developed a dynamic model to predict scaling with $CaCO_3$ and $Mg(OH)_2$ in the MSF condensing tubes and with increasing cooling water temperatures in subsequent stages [56]. Their model was based on a dynamic fouling model for heat transfer surfaces, coupled with an MSF dynamic model to predict the scaling behavior in condensing tubes in the heat recovery section of an MSF plant. First, the deposition rate of either $CaCO_3$ and $Mg(OH)_2$ was found using the diffusion transport rate and surface reaction rate of ions (Figure 7). Total deposition rate is calculated by considering transport of species towards the surface followed by accumulation at the surface, i.e. a combination of diffusion and reaction mechanisms [56]. Transport towards the surface is caused by a concentration gradient between the bulk phase and solid-liquid interface, while accumulation is a result of the concentration difference

between the solid-liquid interface and saturation concentration.

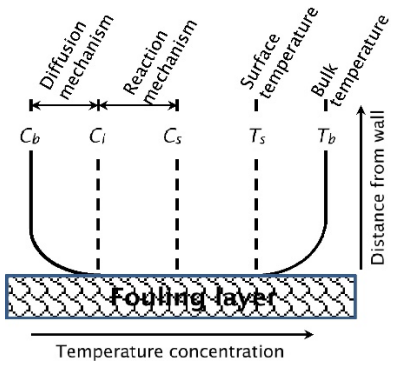

Figure 9: Radial concentration and temperature profiles at heat transfer surfaces [56, 60]; C_b, C_i and Cs are the concentration of ions in the bulk phase, at the solid-liquid surface and the saturation concentration respectively.

They found that lower temperatures favored the deposition of $CaCO_3$, but the slightly increased surface temperature in the middle stages reduced the ratio of Ca to Mg, which in turn favored the formation of $Mg(OH)_2$ in these stages. They found that the resulting varied fouling factor from their dynamic model could lead to a higher performance ratio (Figure 10) and cost reductions, in comparison to typically overestimated values used to design condenser tube surfaces.

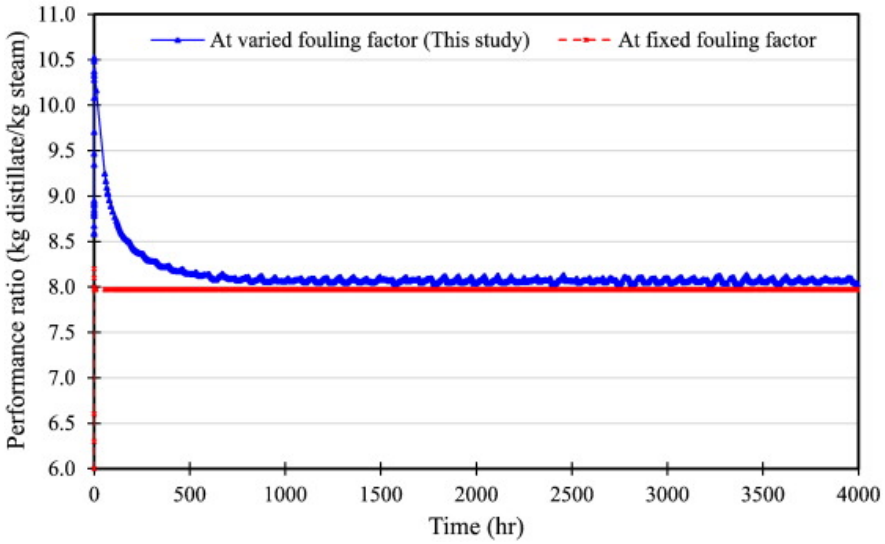

Figure 10: MSF performance ratio for fixed and varied fouling factor [56]

Prevention or mitigation of scale formation in MSF can be achieved by either, 1) adequate pretreatment of the feed to remove scale forming agents, and/or 2) the use of antiscalants to inhibit

the formation of scale [75].

Most pretreatment processes do not involve removal of dissolved solids such as multivalent ions that can later precipitate and cause scaling on heat exchangers, which reduces heat transfer efficiency in both MSF and MED systems. In addition to scale formation, heat transfer surfaces are also affected by the release of non-condensable gases such as carbon dioxide, oxygen, and nitrogen. The presence of CO_2 in the feed stream alters the concentration of HCO_3^-, CO_3^{2-}, CO_2, H^+ and OH^- ions in the brine stream, which in turn affects alkaline scale formation [74]. Nanofiltration has gained importance in the last decade as pretreatment to prevent scale deposition in MSF desalination plants. Nanofiltration can be used to lower the concentration of scale-forming elements in seawater, such as Ca^{2+}, Mg^{2+}, $SO4^{2-}$ and HCO_3^-. After pretreatment with NF, the feed has a significantly lower salinity as NF membranes are capable of not only removing multivalent ions with high efficiency, but can lower the concentration of monovalent ions such as Na^+, Cl^- and K^+. The lower feed salinity resulting from NF pretreatment allows the TBT to increase to 130 °C [76]. The use of NF as pretreatment for thermal desalination systems is not new; both mathematical models [55, 77] and experimental studies [78, 79] on NF/MSF pilot plants shown have shown the efficiency of NF as pretreatment for MSF over the last two decades, demonstrating their ability to reduce scaling and in turn operational costs of the thermal desalination system. Typical models are based on mass transfer and chemical reaction of solutes in the brine, which can be used to calculate scale formation in MSF evaporator tubes. Al-Rawajfeh investigated NF as CO_2 deaerator for thermal desalination systems [74]. Using the mathematical model of mass transfer, they found the molar release rate of CO_2. They simulated the desorption-deposition of CO_2-$CaCO_3$ by mass balance of a differential volume element of liquid at the gas-liquid phase interface. They found that NF pretreatment significantly enhances deaeration (Figure 11) and this decrease in CO_2 release

rates is correlated with lower heat transfer resistances in MSF plants. In addition to reducing scaling potential, the negative effects of CO_2 and other non-condensable gases on heat transfer and vapor-side corrosion are also mitigated when NF is used as pretreatment.

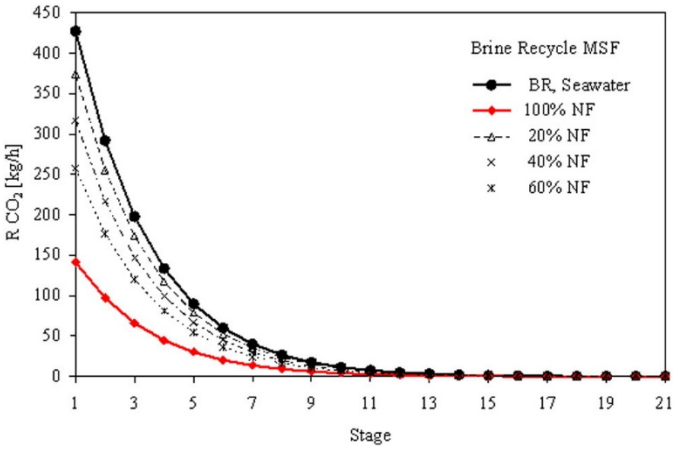

Figure 11: Effect of NF pretreatment on CO_2 release rates in brine recirculation MSF (BR-MSF) [74]

Rawajfeh et al. found that incorporating NF pretreatment with traditional salt precipitation pretreatment allows TBT to reach as high as 175 °C.

2.1.2 Optimization of design and operational parameters in MSF

Hanshik *et al*. used theoretical calculations to indicate that increased TBT led to increased water production which in turn lowers the specific energy consumption (SEC) for a once-through multistage flash (OT-MSF) plant [80]. Figure 12 shows the effect of TBT on the production of desalinated water and on the cooling seawater quality, temperature. However, they did not incorporate any experimental correlation or adjustment for fouling, seawater quality and/or chemical dosing.

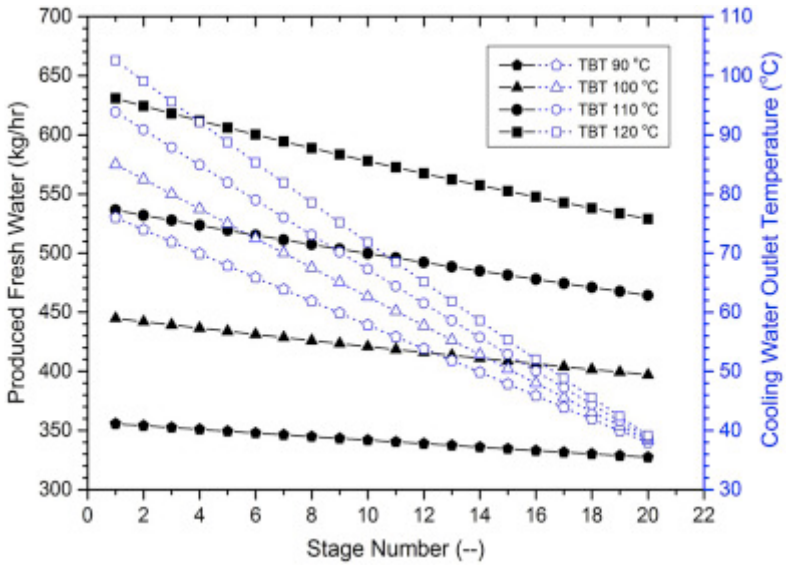

Figure 12: Effect of TBT on freshwater production (solid black lines) and cooling seawater temperature (dotted blue lines) [80]

Roy *et al.* similarly developed a mathematical model to investigate the effect of increasing TBT on the performance of an OT-MSF system, including the required specific area [8]. Unlike Hanshik's work in which a fixed number of stages was studied, they considered a fixed inter-stage temperature drop ΔT and varied the number of stages to increase the TBT. The effect of increasing TBT of up to 160 °C on PR and required specific area is shown in Figure 13. They found that the performance ratio (PR) increases with TBT while the required specific area decreases but then slightly increases beyond a certain TBT. As mentioned in the previous section, a high TBT of 160+ °C and hence improved system performance can be attained by removing scale-forming compounds during pretreatment.

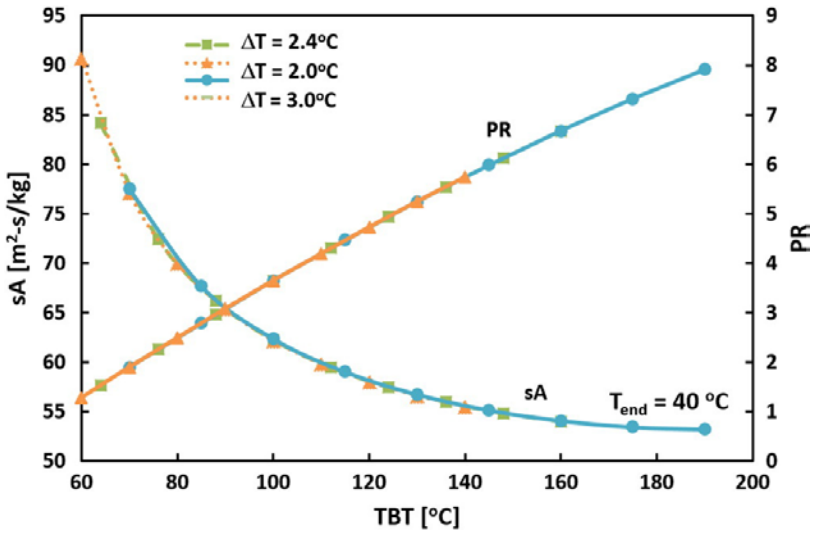

Figure 13: Effect of TBT on specific area and performance ratio in a once-through multistage flash system [8]

Mabrouk et al. demonstrated a 25% reduction in heat transfer surface area by using long tube evaporator bundles as compared to traditional brine recycle and cross tube bundle configurations [55]. In a long tube configuration, the tubes are parallel to the direction of brine flow, whereas in a cross tube configuration, the tubes are perpendicular to the direction of brine flow in the stages (Figure 14).

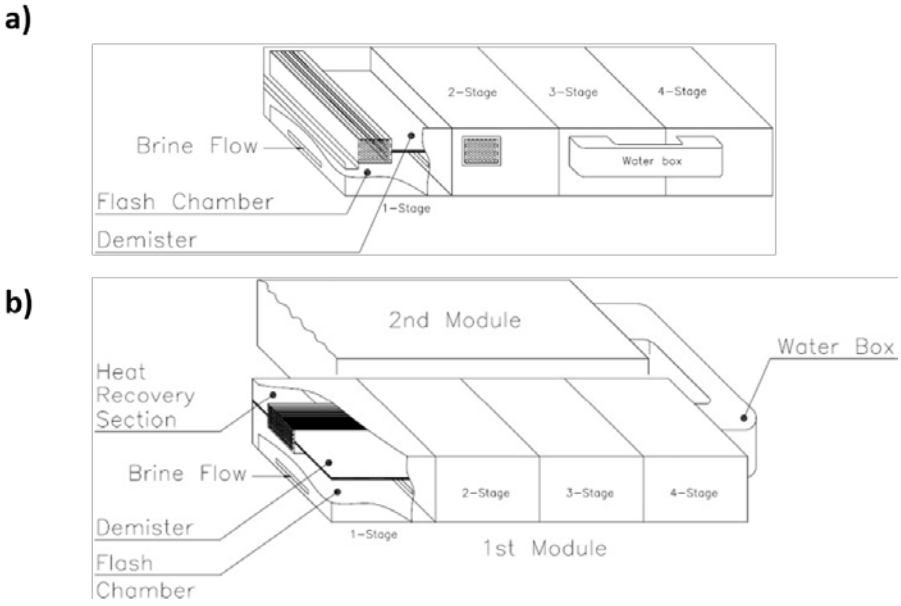

Figure 14: MSF a) cross tube configuration and b) long tube configuration [55]

Their study focused on further scaling up MSF to systems greater than 20 MIGD. They found that

although the operating cost is similar, an MSF system with long tube bundles allows for 15% lower capital cost than its cross tube counterpart, for a large scale project of 100 MIGD.

Ben Ali and Kairouani optimized operating parameters of a brine recirculation MSF plant [81], considering changes in brine heater fouling factor and the seasonal variation in seawater temperature using genetic alogrithms used to solve multi-objective optimization problems. The operating parameters that were optimized were heating steam temperature (T_{hs}), recycled brine flow rate (M_R), cooling seawater flowrate (M_{CW}) and make-up seawater flow rate (M_f). The plant data used includes 16 flashing stages and a nominal production capacity of 26,700 m^3/day. The objectives were to maximize fresh water production capacity, minimize thermal energy consumption by reducing heating steam flow rate and minimize electrical energy consumption by minimizing flow rates from pumps. They obtained a set of Pareto optimal solutions in which combinations of optimal operating parameters were defined. To solve the optimization problem, they used a steady-state process model of the plant, which consisted of mass and energy balances and heat transfer equations.

They found that, for a constant T_{hs}, M_{cw}, M_R and M_f, fresh water production decreases as seawater temperature rises and although the fouling factor decreases continuously, its effect on water production capacity is less pronounced. This can be observed in Figure 15, where between April and November, the fouling factor increased by 90.7% but fresh water production declined only by 2.2%.

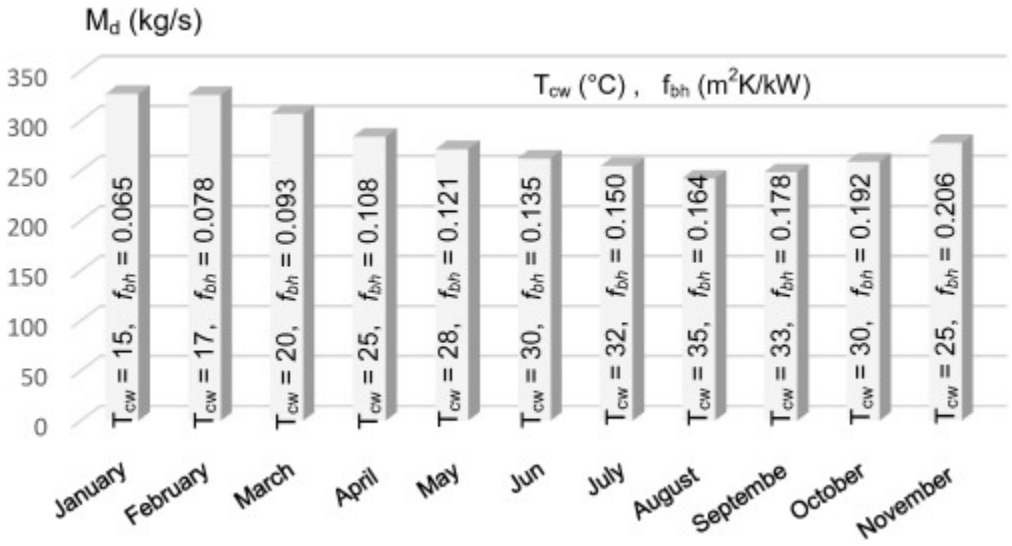

Figure 15: Variation of plant production capacity as a function of seawater temperature and brine heating fouling factor (T_{hs} = 93 °C, M_{cw} = M_R = M_f = 1500 kg/s) [81]

Improvements in configuration have led to significant cost reductions in MSF. The simplest design, known as once-through MSF (OT-MSF), involves returning the brine leaving the last stage back to the sea as brine blow down. The brine leaving the last stage of the MSF can be returned to the sea as brine blow down, a configuration known as once through MSF (MSF-OT). Another configuration which is known as brine mixing MSF (BM-MSF) involves mixing a portion of the brine from the last stage with the incoming feed. Dahdah and Mitsos sought to optimize brine and feed routing by developing a superstructure representing thermal desalination structures [82]. This enabled them to perform optimization studies on various MSF configurations.

Bandi et al. [83] adopted a differential evolution (DE) algorithm to address the global optimal design of MSF systems. They use non-linear programming (NLP) based process models together with non-deterministic optimization algorithm to evaluate MSF-OT, MSF-simple mixture (MSF-M) and MSF-brine recycle (MSF-BR) configurations, and compared obtained solutions with those obtained with MATLAB. A non-deterministic algorithm differs from traditional algorithms in that it can arrive at outcomes using various routes, or that, even for the same input, can exhibit different behaviors for different runs [84]. Bandi et al. use freshwater production cost as the objective

function for minimization, constraints are imposed by mass, energy and enthalpy balances. They found that the obtained global solution from DE is >2% better than from other deterministic optimization algorithms such as SQP, MS-SQP and DE-SQP. In the latter, the optimal variable value set and objective function depend on the initial gas value, whereas DE provides better initialization strategies and is more suitable for complex problems in terms of decision variables. Figure 16 shows how the different optimization methods differ in terms of optimal cost obtained for all three MSF configurations.

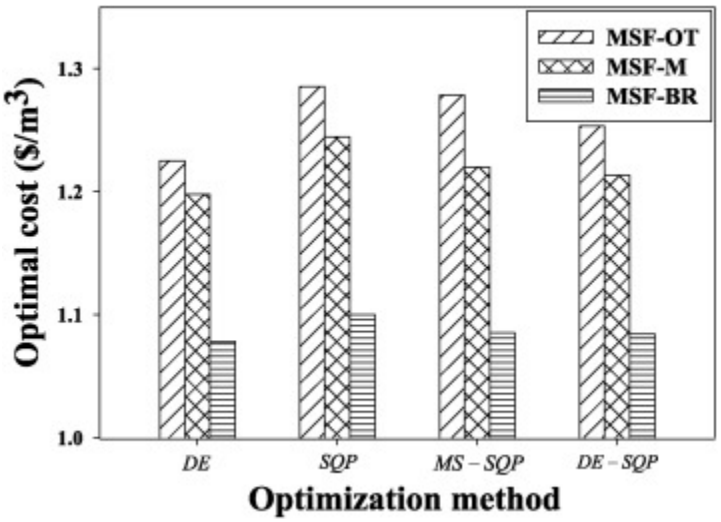

Figure 16: Comparison of different optimization methods used to minimize fresh water production costs in MSF-OT, MSF-M [83]

Selected design parameters and their effect on MSF performance are shown in Table 2.

Table 2: Selected operation and design parameters and their effect on MSF performance

Parameter	Effect	Reference
TBT	Increasing TBT increases water production, lowers specific energy consumption, lowers reduced specific area and increases performance	[8, 80]

	ratio	
Configuration of evaporator bundle	Long tube evaporator bundle lowers heat transfer area	[55]
Seawater temperature	Increased seawater temperature decreases production water capacity	[81]

2.2 Optimization modelling in membrane processes

2.2.1 Reverse osmosis

2.2.1.1 Mathematical modelling in RO

The solution diffusion model, developed in the 1960s, remains the most commonly used model to describe transport through an RO membrane is the solution diffusion model (Figure 17). In this model, transfer of the solvent (water) and the solute (salt) through a non-porous membrane occurs in three steps: absorption to the membrane, diffusion through the membrane and desorption from the membrane [18]. The driving force is the chemical potential gradient such that when the applied hydrostatic pressure is greater than the difference in osmotic pressure between both sides of the membrane, water is transported through against its natural flow due to difference in chemical potential.

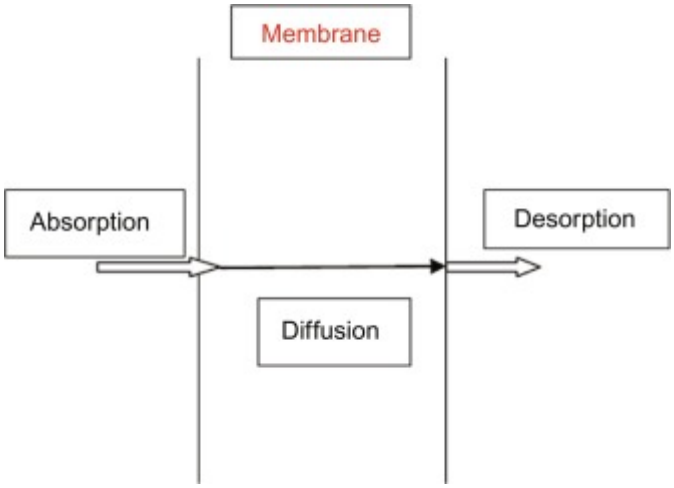

Figure 17: Solution-diffusion model for RO membrane [18]

In the solution diffusion model, salt and water flux are given by:

$$J_w = A_m(\Delta P - \Delta\pi)$$

$$J_s = B(C_w - C_p)$$

where osmotic pressure is obtained from the van't Hoff equation.

Although there has traditionally been little evidence on the presence of pores in RO membranes due to measurement limitations, gradually strengthening the support for the solution-diffusion model over the decades, some pore-based models also emerged [85-87], which are now being supported by experimental data as measurement tools for sub-nanometer pores become advanced, as discussed by Ismail et al. [18, 88].

Early on, Starov's group developed a model to investigate RO for multicomponent electrolyte solutions [89-91], in which they applied extended Nernst-Plank equations to include diffusion, confection and electromigration of ions. In their model, the boundary conditions included both (i) distribution coefficients for individual ions, determined by specific interaction of ions and membrane material, and (ii) electric potential jump at the feed solution-active layer interface, known as Donnan potential. The model incorporates a mechanism for varying membrane fixed charge as a function of ion concentration and pH inside the active layer of the membrane. In

addition to sodium and chloride ions, hydrogen and hydroxide ions are also also taken into consideration. In [90], a method of calculations of rejections of multicomponent of electrolyte solutions was developed, which allowed prediction of rejection coefficients of all ions in the mixture as functions of both salt concentrations and pH based on experiments with individual salts (Figure 15), which was then verified in [89], showing a reasonable agreement between theoretical predictions and experimental measurements.

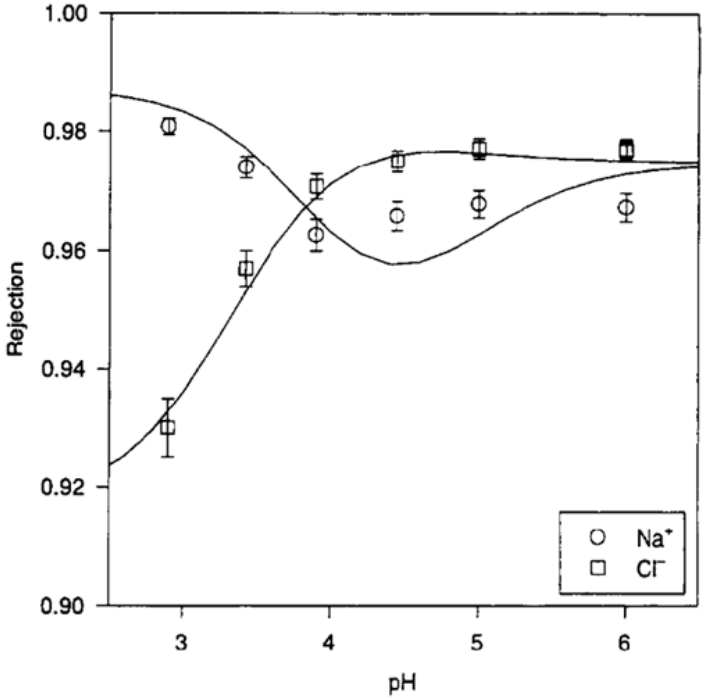

Figure 18: Rejection vs. pH for a feed concentration of 6 x 10^{-4} M NaCl solution. Solid line according to the theory predictions [89]. The membrane used was Osmonics SS10 cellulose acetate membrane.

Recently, Shen et al. apply non-equilibrium molecular dynamics to relate water transport to the membrane structure for RO, arguing that existing models rely on macroscale assumptions and do not provide a molecular level understanding of transport in an RO membrane [92]. Interestingly, they found that membranes with similar density and tortuous paths differed in water transport, which correlates with the percolated free volume through the membrane thickness. Molecular collisions alter the structure of the membrane under hydration which also has an effect on the

transport of water molecules. They suggested that solute transport could correspond to its bonding with the functional groups of the membrane and/or its hydrating solvation shell.

2.2.1.2 Optimization modelling in RO

Energy consumption, which represents more than 50-60% of total costs in desalination [93], is the key determining factor in the widespread employment of any technology. On the energy front, seawater reverse osmosis (SWRO) is a mature technology in which energy-efficient membranes and energy recovery devices (ERDs) are employed and lead to significantly lower energy consumption as compared to thermal desalination [94]. Theoretical energy consumption in RO is 0.77 kWh/m^3, while for thermal desalination it is 709 kWh/m^3.

In the 1970s, RO consumption was over 15 kWh/m^3 of water produced. Currently, RO consumes as low as 2 kWh/m^3. As a whole, RO plants today consume 2.5-5 kWh/m^3 of water produced [93]. This drastic reduction in overall energy consumption is a result of lower energy consumption in each of the components making up the RO plant. These include the pretreatment system, high pressure pumps, membrane material, membrane configuration, energy recovery devices (ERDs), and post-treatment. In a recent review, Zarzo and Prats discuss strategies for minimizing energy consumption in RO plants [93].

As RO technology is already running very close to its theoretical energy consumption, research focus has shifted to improving system design, optimizing pre- and post-treatment, integrating RO with other desalination processes and/or renewable energy sources [95, 96].

SWRO specific energy consumption can be further reduced through improvements in RO design configurations. Performance of new design configurations is first optimized using simulations before lab-scale experiments are carried out to validate results. As such, modelling tools are crucial to the development of energy-efficient process designs, because they provide a facile tool for

process optimization without the need for pilot testing. The configuration of RO membranes inside pressure vessels has been the focus of recent studies aimed at reducing energy consumption, especially for seawater reverse osmosis (SWRO). Part of the driving force is the tradeoff between membrane selectivity and permeability [97]. Membranes with high selectivity may separate salt efficiently, but the low water transport results in high SEC. On the other hand, high-flux membranes have higher water production, but also a greater tendency to foul [94]. Lin and Elimelech compared SSRO, two-stage RO and CC-RO in terms of specific energy consumption and average water flux [98] as an indication of RO mass transfer energetics and kinetics, respectively. In the single stage process, the feed stream is split into brine and permeate streams as it passes through the RO membrane. In a two-stage RO process, the brine stream of the first stage becomes the feed to the second stage and permeate streams of both stages are collected. In a CC RO system, the brine is mixed with the feed solution and sent through the membrane (Figure 15).

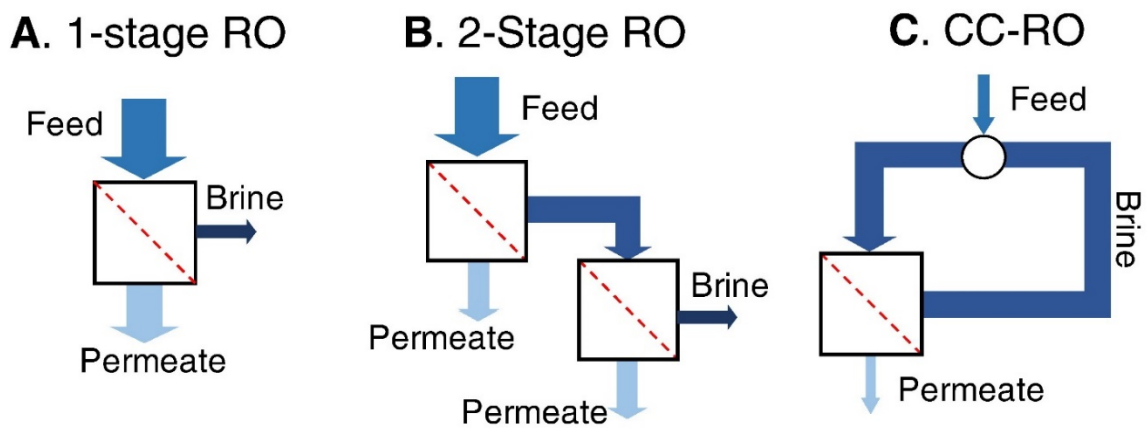

Figure 19: Schematic showing A) Single stage RO (SSRO), B) Two-stage RO and C) Closed-circuit (CC) RO [98]

Their results show that a CC-RO is less energy-efficient than a two-stage RO process due to the extra energy required to reduce the entropy generated by the mixing of the feed and retentate [26]. A two-stage RO also yields a higher water flux for brackish water desalination, where the recovery

rate is typically high (90%) [98].

Although energy efficiency can be enhanced by adding more stages, the additional capital costs associated with adding a stage outweigh the reduction in energy costs [99]. Other configurations and routing of the brine and permeate are also necessary to bring about improvements in energy efficiency and costs. Recently, Chong and Krantz [100] developed an energy-efficient reverse osmosis (EERO) system in which they sought to increase overall water recovery by sending the retentate from one or more SSRO as feed to a countercurrent membrane cascade with recycle (CMCR), consisting of one or more low salt-rejection RO stages (Stage 1) and a high salt-rejection stages (Stage 2) (Figure 16). In EERO, the retentate from an SSRO is sent to a two-stage CMCR. Along with retentate reflux in Stage 1, the countercurrent flow of the retentate and permeate streams result in lower osmotic pressure differential and therefore lower net specific energy consumption [100]. By using EERO, an overall water recovery of 75% can be attained at a cost lower than SSRO operating at 50% water recovery.

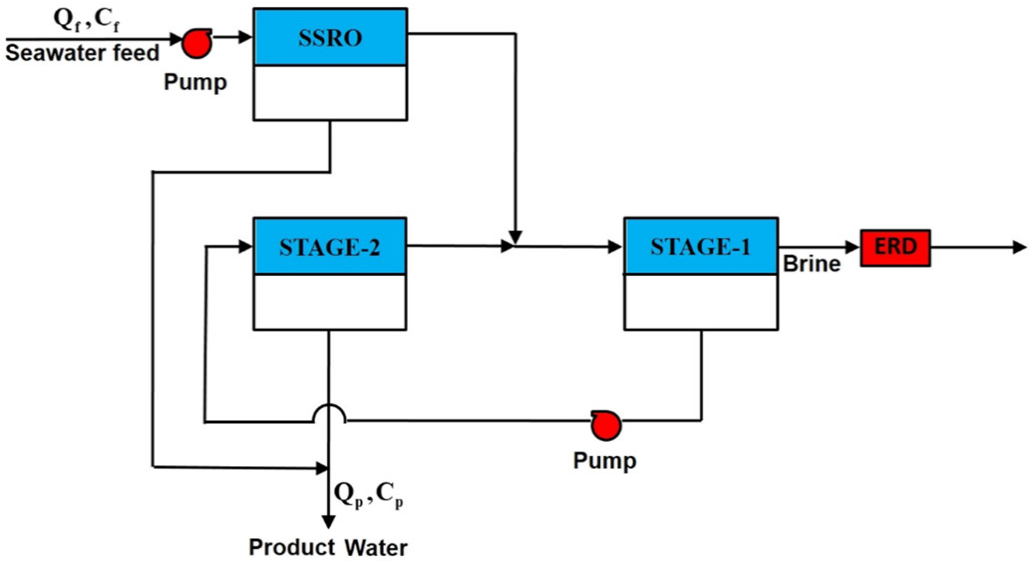

Figure 20: Schematic of EERO process in which retentate from SSRO is sent to a two-stage CMCR [100]

In a later study focusing on the numerical model-based analysis of the EERO system [99], Chong's group evaluated the fouling potential of the EERO system. As shown in Figure 17, the elements

in the EERO modules maintained a lower flux. This is especially true for the lead elements and can be significant in mitigating the effects of membrane fouling in these elements, as well as increasing water recovery rates.

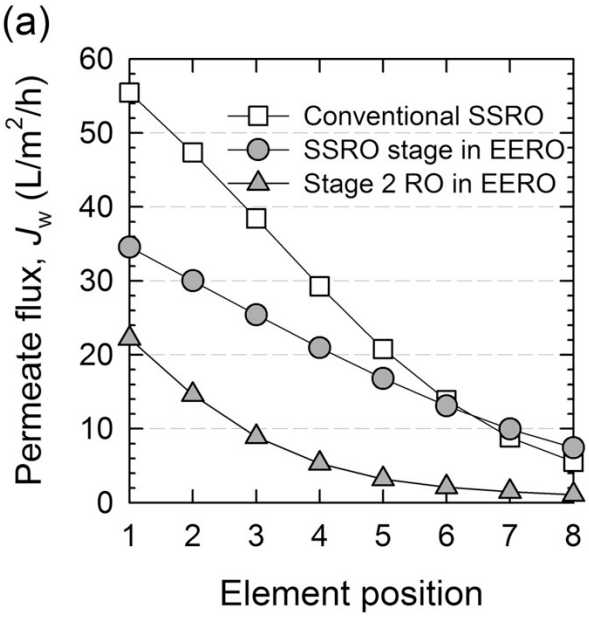

Figure 21: Permeate flux J_w of an RO stage in conventional SSRO and EERO processes (simulated at 60% overall water recovery) [99]

Kim and Hong introduced split partial single pass RO (SSP-RO) configuration in which the permeate from only the back RO elements in a pressure vessel is blended with the feed to RO in order to dilute the feed [101]. This results in high-quality permeate with lower energy demand. They modelled the process and found that energy efficiency is maximized for the SSP RO process when the permeate from the last element is blended with the feed. Compared to conventional single-pass RO, the permeate from the modified process was 15% greater in purity and more energy efficient than two-pass RO, in any case.

Typical configuration of a single stage RO applies the same membrane type throughout a pressure vessel. This causes the front elements to be exposed to the feed seawater, resulting in a higher net pressure difference and higher flux across these elements in comparison to subsequent elements.

This uneven distribution of net driving force also results in greater propensity to foul for the front elements. An improvement of the process design aimed at making the flux distribution along a pressure vessel more uniform, is to use a hybrid membrane configuration, known as internally staged design (ISD). ISD involves using lower flux membranes at the front and high flux membranes in subsequent elements (Figure 18) [102, 103]. It has been shown that such a hybrid membrane inter-stage design has the potential for significant reductions in permeate costs by requiring fewer pressure vessels and membranes [104, 105]. This section covers optimization of ISD and other such developments in RO membrane configurations using modelling and simulation over the last 5 years.

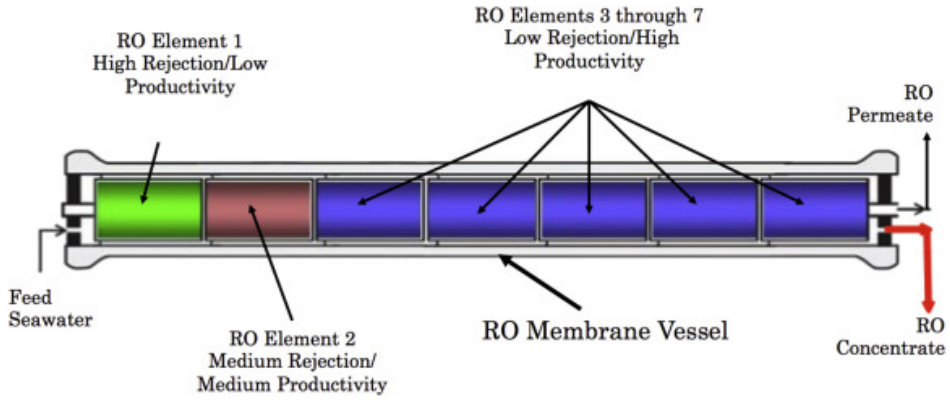

Figure 22: Schematic showing a hybrid membrane configuration, or internally staged design (ISD) [102]

Jeong et al. developed a finite difference model to numerically optimize ISD in the presence of colloidal foulants [106]. They numerically modeled transport phenomena in a full-scale RO membrane process and investigated the impact of the membrane element arrangement on long-term operation (Figure 19) [106]. Compared to conventional designs where the same membrane is incorporated throughout the vessel, the ISD resulted in greater water flux and higher energy efficiency for long-term operation, without compromising on the quality of the permeate (< 400 mg/L). They applied finite difference approximation to numerically calculate the spatial and temporal distribution of water and solute transport. This is done by discretizing the spatial domain

x into 100 finite elements and time on a daily basis over a period of 90 days. Salt and water fluxes over each segment were calculated from the first to the last membrane element at a given time step. Model parameters for calculation of the cake layer growth are updated based on those of the previous time step and then applied to the equations for steady-state mass transfer. Similar recursive algorithms have been used to predict fouling in other studies as well [107-111].

In a full-scale RO process, four to eight RO elements are connected in series in a single pressure vessel and each membrane's performance varies depending on the temporal and spatial variation in local fluid conditions. For an accurate calculation of local water and solute fluxes, they considered the spatial distribution of cross-flow velocity, solute concentration, and trans-membrane hydraulic pressure.

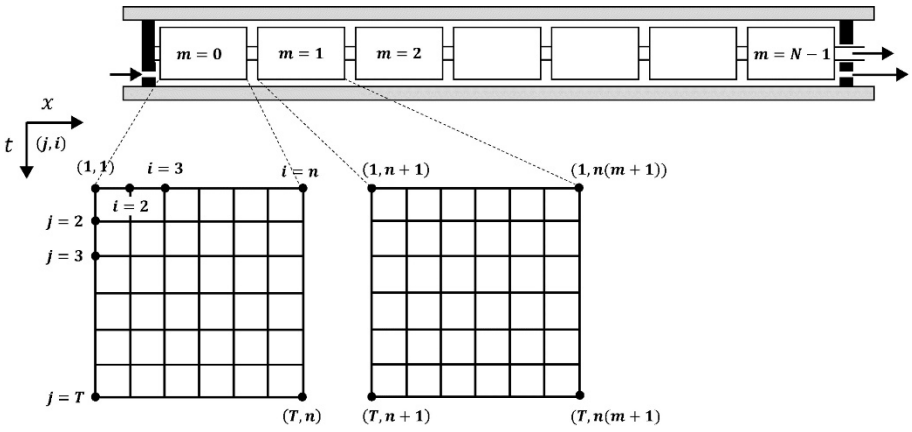

Figure 23: Schematic of RO process illustrating discrete spatial and time domains for numerical calculations [106]

Han et al. improved vessel design by implementing ISD on a single-pass SWRO design and evaluated the effect of configuration on SEC, permeate water quality, and boron rejection [103] using ROSA9, the commercial simulation program provided by Dow Water and Process Solutions. They used three types of RO membranes: high rejection, standard, and high flux membranes (Table 3) in standard configuration and six ISD configurations (Table 4) in a single stage single pass RO system. They found that using an HID configuration with 3 standard membranes in the front and 4 high flux membranes in the tail saves 0.41 kWh/m^3 for the same recovery rate and feed conditions

[103].

Table 3: Specifications of selected SWRO membranes used by Han et al. [103] (32,000 ppm NaCl, 800 psi, 25 °C).

Membrane	Flow (GPD (m^3/d))	Salt rejection (%)	Boron rejection (%)	Type
SW30XHR-400i	6000 (22.7)	99.82	93	High rejection
SW30HRLE-400i	7500 (28.4)	99.8	92	Standard
SW30ULE-400i	11,000 (41.6)	99.7	89	High flux

Table 4: Membrane configurations used by Han et al. [103]

Configuration	Membrane element
XHR	SW30XHR-400i
HRLE	SW30HRLE-400i
ULE	SW30ULE-400i
HID 1	(SW30XHR-400i) 3 + (SW30HRLE-400i) 4
HID 2	(SW30XHR-400i) 3 + (SW30ULE-400i) 4
HID 3	(SW30HRLE-400i) 3 + (SW30XHR-400i) 4
HID 4	(SW30HRLE-400i) 3 + (SW30ULE-400i) 4

Configuration	Membrane element
HID 5	(SW30ULE-400i) 3 + (SW30XHR-400i) 4
HID 6	(SW30ULE-400i) 3 + (SW30HRLE-400i) 4

Optimal design of RO units has been the focus of considerable research. According to Kotb *et al.*, most of these optimization studies involve complex models or highly nonlinear equations with many constraints [112]. In their recent study, they implemented a simple transport model to determine the operating parameters corresponding to optimum RO system structure i.e. single, two, and three-stage arrangements with respect to minimum permeate production cost for a given permeate flow rate with defined maximum total dissolved solids (TDS) [112]. They found that the minimum overall cost per unit permeate for a three-stage system is 0.91 $/m^3 produced at a rate of 17 m^3/h.

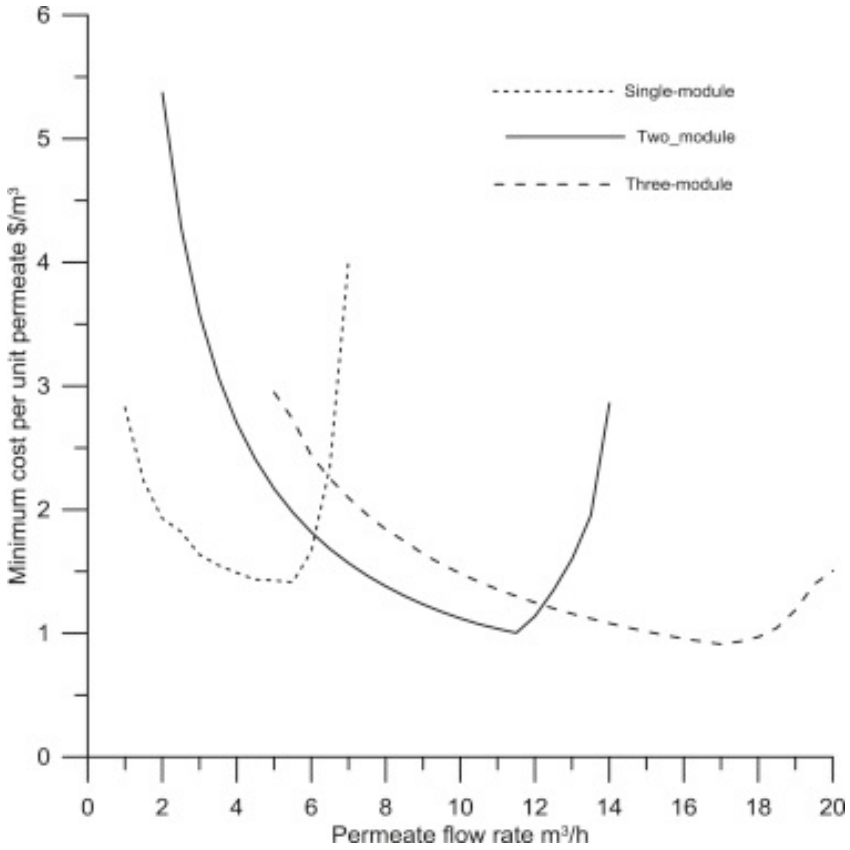

Figure 24: Effect of permeate flow rate on minimum cost per unit permeate $/m^3 for single module, two-stage and three-stage modules [112]

Figure 20 suggest that the optimum permeate flow rate increases with the number of stages, indicating that while a single-stage RO system is suitable for up to 6 m^3/h, three-stage modules are suitable for production up to 20 m^3/h.

Obaidi et al. [113] optimized a two-stage/two-pass RO process for chlorophenol removal from wastewater and found that they could increase rejection by 12.4% compared to SSRO, for a 40% recovery rate, while keeping energy consumption at 1.949 kWh/m^3.

The cake filtration mechanism used to describe particulate fouling on the surface of NF and RO membranes is extensively covered in literature [114]. Cake filtration models are often used when scaling, pore blocking, and biofouling are not major contributors to fouling.

Tomaszewska et al. [115] used empirical equations and numerical modelling to formulate trends on the membrane surface and, thus, to predict membrane scaling during RO. Numerical modelling

takes into account operating conditions as well as physicochemical properties of the feedwater with and without antiscalants. In comparison to traditionally used methods to predict scaling such as RSI and LSI, the model suggested in this study predicts scaling phenomena as well as reactions between water and antiscalants. Table 5 shows the expressions for calculation of water flux and net SEC for different RO configurations.

Table 5: Expressions for average water flux and net SEC for selected RO configurations

System configuration	Average water flux $\overline{Jw}$	Specific energy consumption	Ref.
Single-stage RO (SSRO)	$\frac{\alpha^2 RR}{\alpha R + ln\left(\frac{\alpha - 1}{\alpha(1 - RR) - 1}\right)}$	$\frac{1}{1 - RR} + \varepsilon$	[98]
Two-stage RO	$\frac{1}{N_{RO,2S(}RR, RR_1, \alpha_1\alpha_2)}$	$\frac{RR_1}{RR}\alpha_1 + \frac{RR - RR_1}{RR}\alpha_2$	[98]
Closed-circuit RO (CCRO)	$\frac{\emptyset}{N}\frac{1}{ln(1 + \frac{\emptyset}{N\varepsilon})}$	$1 + \varepsilon + \frac{N + 1}{2N}$	[98]
SSP RO	$A_m * TCF[(Pb - Pp) - CPF\ \pi_b - \pi_p)$*	$\frac{\frac{1}{36}\sum\frac{\Delta P_{device} Q_{f,device}}{\eta_{device}}}{Q_{p,sys}}$	[101]
EERO (3-stage)	-	$\left[1 + \frac{1 - RR_{SSRO}}{RR_2(1 - RR_2 + RR_{SSRO}}\right]\frac{\Delta\pi}{\eta_{pump}} - \left[\frac{1 - RR_{SSRO}}{RR_{SSRO} + (1 - RR_2)}\right]\eta_{ERD}\Delta\pi$	[99, 100]

*TCF = $\exp\left[\frac{e}{R}\left(\frac{1}{298} - \frac{1}{273+T}\right)\right]$

Khayet et al. [116] used response surface methodology (RSM) and ANN to develop predictive models for RO desalination. They used a polyamide thin film composite membrane in spiral wound configuration, with aqueous NaCl solutions as model feed solutions and developed the models

based on experimental designs. The input variables for their model were NaCl concentration in feed, feed temperature T, feed flow-rate Q and operating hydrostatic pressure P. RSM is an optimization approach that allows combination of several input factors to optimize a given objective function [117], which in this case is the RO performance index given by salt rejection factor x permeate flux. Response surface models involve fitting a polynomial regression model using the input variables to determine the critical point, i.e. maximum performance index. On the other hand, ANN is a non-linear processing system in which neurons, or nodes, and connections between them are used for mapping input and output data [118]. A neuron is a computational processor which operates in conjunction to other neurons such that the connections are characterized by weights and biases. It was discovered that a single RSM model could not adequately predict the performance index over a wide range of salt concentration (for both brackish and seawater desalination conditions). They found that pressure played an important role at higher feed temperatures and the feed temperature was an important factor at higher operating pressures. The optimal conditions found through ANN were better than those by RSM [116] and the predicted values from ANN closely fit experimental data with a correlation coefficient close to unity, as shown in Figure 25. This was attributed to selection of optimal ANN architecture and other factors.

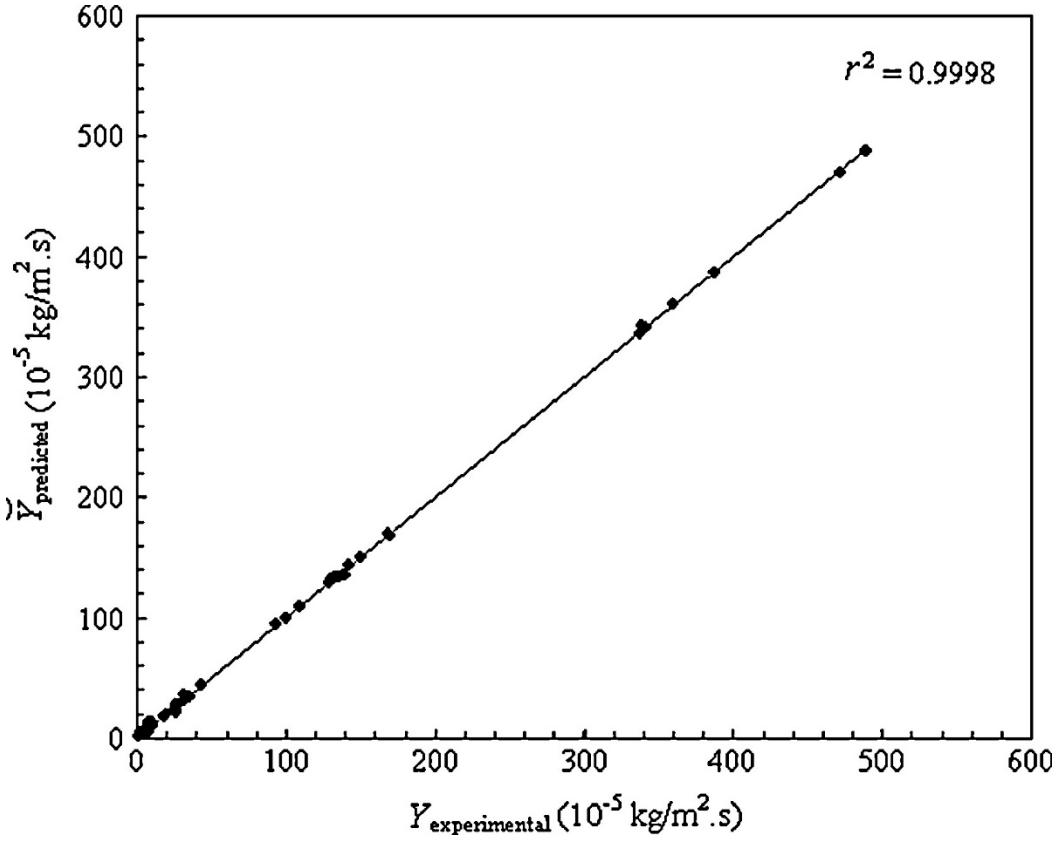

Figure 25: RO performance index predicted by ANN vs. experimental values [116]

2.2.2 Mathematical modelling in nanofiltration

Due to the complexity of modelling transport and separation, especially of charged solutes, many studies have focused on NF modelling in the last two decades [50, 119]. In this section, theories pertaining to ion transport and fouling in NF are considered, and existing models are connected with technological application of NF in desalination.

There are several models describing transport through NF membranes, including irreversible thermodynamic models, pore models, space charge models, electrostatic, and steric-hindrance models [49, 120]. A summary of commonly used ion transport models in NF is shown in Table 76, and described in detail in [30, 49]. Modified versions of these models are used to describe separation of more complex solutions with NF, such as mixed salt solution [49]. Physical sieving is the dominant mechanism for rejection of large molecules and solutes, whereas the chemistries

of solute and membrane take precedence for ions and low molecular weight organics. In most models, the membrane is assumed to be a bundle of charged capillaries with specific structural parameters, namely pore radius r_p, with a ratio of porosity to membrane thickness (ε/l) and surface charge density.

Ion transport in NF is described either by two kinds of models: irreversible thermodynamics models, in which the membrane structure is not considered and transport is described as an irreversible process which continuously produces entropy and dissipates free energy, or models in which the structural and physiochemical properties of the membrane dictate solute transport such as steric-hindrance pore model and Teorell-Meyer-Sievers (TMS) model.

Kedem-Katchalsky and Spiegler-Kedem models are non-equilibrium thermodynamic models in which the solute flux is a function of solute permeability coefficient P_i, average solute concentration in the membrane $\bar{c}_i$, solvent permeability coefficient L_p, permeation pressure Δp, reflection coefficient σ_i (corresponding to the solute fraction rejected by the membrane), and the osmotic pressure difference $\Delta\pi$ of water across the membrane.

In the Kedem-Katchalsky model, which is the first irreversible thermodynamic-based membrane model, the solvent flux J_j and solute flux J_i of aqueous solutions containing a single solute are expressed by:

$$J_j = L_p(\Delta p - \sigma_i \Delta\pi)$$

$$J_i = P_i \Delta c_i + (1 - \sigma_i) J_j \bar{c}_i)$$

Both diffusion and convection contribute to solute transport. Diffusion depends on solute concentration while convection depends on the applied pressure. Retention then is dependent not only on the flux but also on the solute concentration. The Spiegler-Kedem model expresses solute flux in a differential form, when the concentration difference between retentate and permeate is

high.

This model was modified by Spiegler and Kedem, who expressed the solute flux Ji as:

$$J_i = -P'(\frac{dc_i}{dx}) + (1 - \sigma_i)J_j\bar{c}_i)$$

where P' is the local solute permeability ($P' = P_i\Delta x$). In this model, the solute permeability coefficient and the reflection coefficient are obtained by fitting observed solute rejection R vs. flux F, according to:

$$R = \frac{\sigma_i(1-F)}{1-\sigma_i F}, \text{ where } F = \exp\left(-\frac{1-\sigma_i}{P_i}\right)J_j$$

The retention coefficient which corresponds to the maximum rejection at infinite volume flux can be determined by fitting of experimental data of rejection as a function of flux. These thermodynamic models require less information to set up and have been used to describe the rejection behavior of many solutes. The limitation of using thermodynamic models is that less information is extracted about transport through the membrane.

Another kind of model involving porous membranes is the steric-hindrance pore (SHP) model. In this model, separation is described in terms of membrane pore radius and the ratio of membrane porosity to thickness (ε/*l*). For a system containing a single uncharged solute, the reflection coefficient and the solute permeability coefficient can be expressed in terms of steric parameters related to the wall correction factors in the convection and diffusion coefficients, as well as to the distribution coefficients of solute in the convection and diffusion conditions.

$$\sigma_i = 1 - H_F S_F$$

$$P_i = H_D S_D D_i(\frac{\varepsilon}{l})$$

Where H_F and H_D are steric parameters related to the wall correction factors in the convection and diffusion coefficients, respectively, and S_F and S_D are the distribution coefficients of solute in the

convection and diffusion conditions, respectively. Another equation widely applied to describe pure solvent flux through uniform cylindrical pores without any concentration gradient across the membrane is the Hagen-Poiseuille equation:

$$J_j = \frac{\varepsilon r_p^2 \Delta P}{8\mu\tau l}$$

where μ is the solvent viscosity and ε, r_p, l and τ are membrane porosity, pore radius, membrane thickness, and tortuosity factor, respectively.

The Teorell-Meyer-Sievers (TMS) model, also known as the fixed-charge model, relates salt rejection by charged membranes to the ratio of membrane effective charge density to feed concentration. The TMS model, which is based on the Donnan equilibrium theory and the extended Nernst-Planck equation, assumes a homogeneous membrane with a uniform distribution of potential and concentration [119, 121]. Donnan equilibrium theory describes the behavior of charged particles near a semi-permeable membrane wherein some ions are retained by the membrane to maintain electroneutrality on each side [122].

Built on the extended Nernst-Planck equation, the Donnan steric pore-flow model (DSPM) is widely used to describe ion transport in NF. In addition to the sieving effect, this model also takes into consideration ion transport in terms of diffusion and migration, resulting from concentration and electrical potential gradients, as well as convection due to the pressure difference across the membrane [30]. In the DSPM, the membrane is considered a charged porous layer in which the pore radius, volumetric charge density, and effective membrane thickness are controllable parameters [123]. It describes partitioning through steric hindrance and the Donnan equilibrium theory.

Table 6: Commonly used transport models for NF membranes [30]

Model	**Transport mechanism**

Kedem-Katchalsky model	Diffusion and convection
Spiegler-Kedem model	Diffusion and convection
Hagen-Poiseuille model	Convection
Steric hindrance pore model	Convection
Teorell-Meyer-Sievers (TMS) model	Electrostatic interactions
Donnan steric pore-flow model (DSPM)	Diffusion, convection, and electrostatic interactions

Now that key transport models for NF have been discussed, the present section reviews new models as well as improvements of existing NF transport models that have been developed in the last five years.

Kowalik-Klimczak [124] evaluated the DSPM model for analyzing NF for the removal of chromium(III) ions from an acidic salt solution. The pore dielectric constant was identified by testing at different pressures and feed compositions. The permeate flux values obtained from the model were in agreement with experimental values (Figure 26).

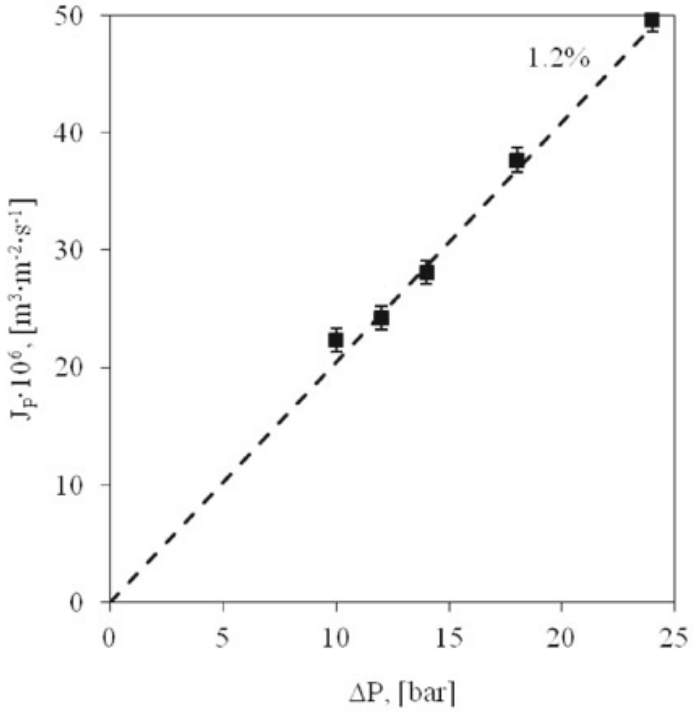

Figure 26: Permeate flux (Jj) vs. transmembrane pressure for feed consisting of 2 g Cr^{3+} dm^{-3}, 10 g Cl^- dm^{-3}, 10 g $SO4^{2-}$ dm^{-3} (the dotted line shows the pore model fitted to experimental values) [124]

Kong et al. employed the DSPM and dielectric exclusion model to predict the performance of two NF membranes for the rejection of six haloacetic acids (HAA) and six pharmaceuticals (PhACs) with different molecular weight, hydrophobicity, and charge [125]. Their model could predict the rejection of HAAs with a mean standard error less than 5%. However, the model overestimates the rejection of PhACs. This is because even though the model cites diffusion as the predominant mass transport mechanism, experiments show that diffusion had a much smaller contribution. The disagreement of model predictions and experimental values is possibly due to inappropriate quantification of the hindrance factors for convection and diffusion, i.e., H_D and H_F. Abdellah et al. applied NF for the recovery of bio-derived solvents from binary mixtures with canola oil [126]. They used Maxwell-Stefan formulations together with Flory-Huggins solubility model to describe the flux data as a function of concentration, feed temperature, transmembrane pressure, and cross-flow velocity (Figure 27).

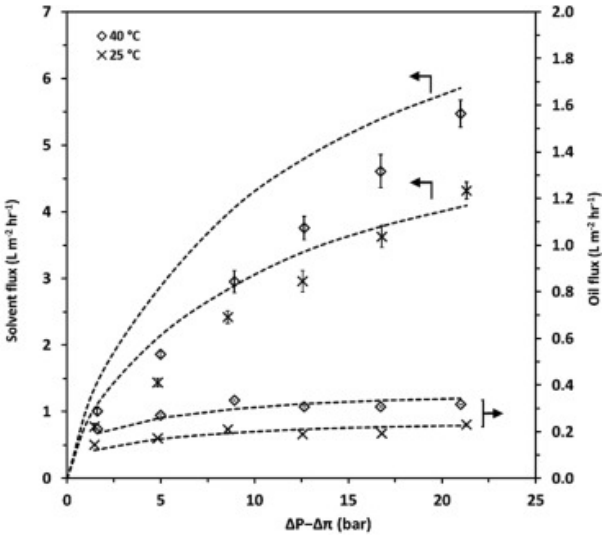

Figure 27: Flux of pinene and oil through PDMS/PAN membrane from 10 wt. % oil mixtures; symbols represent experimental data; lines are simulation results [126]

Labban et al. applied the Donnan-Steric pore model with dielectric exclusion (DSPM-DE) to describe membrane performance for a low pressure NF softening process [119]. They validated the model by comparing with experiments of various feed chemistries including uncharged solutes, single salts, salt mixtures and artificial seawater to characterize and predict its performance. Using the model, they found that the high rejection of NF membranes to multivalent ions results from primarily the membrane pore dielectric constant, followed by pore size (Figure 28). Membrane charge density and membrane thickness were not as crucial in determining rejection for softening applications.

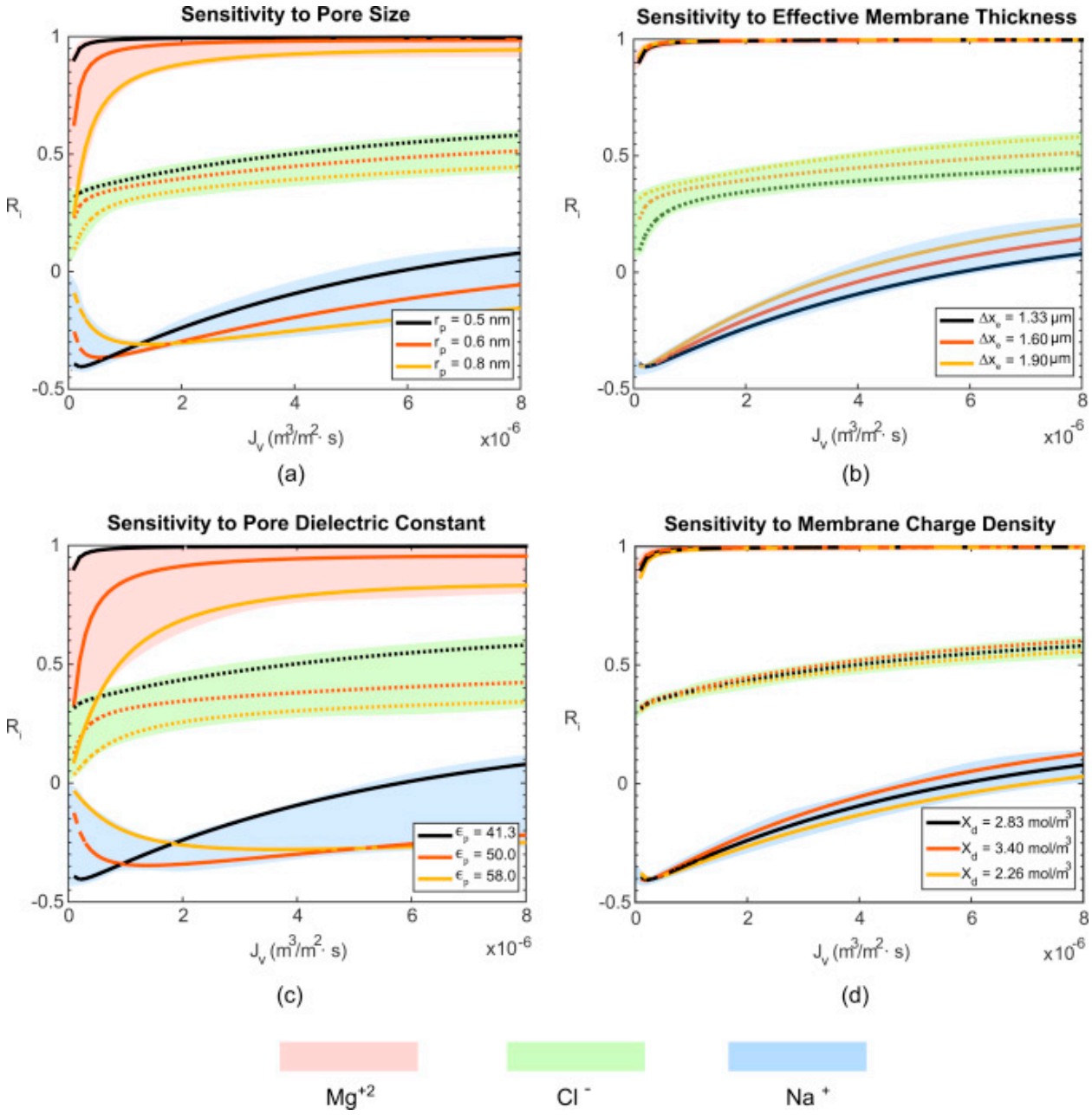

Figure 28: Sensitivity of NF salt rejection for low pressure softening to intrinsic membrane properties [119]

Ochando-Pulido applied a boundary flux theory to model the performance of and predict the fouling in NF for purification of olive mill wastewater after pretreatment [127]. The boundary flux concept is a combination of critical and threshold flux and is a direct function of time [128]. It separates membrane operation into two regions: one in which the impact of fouling is very low and another in which fouling builds up exponentially [127]. Critical flux theory has been used to

describe the maximum permeate flux before fouling occurs, and it has been a crucial component in membrane process design for all processes [129, 130]. An alternative concept, the threshold flux, then emerged as the flux that separates a low fouling region from a high fouling region [130, 131], and was subsequently used to model fouling where critical flux was not applicable. In their work, Ochando-Pulido estimate the boundary flux through by determining the fouling parameter in each region. The experimental flux decline was in agreement with the boundary flux model developed. They found that a high permeate productivity of up to 68.2 L m^{-2} h^{-1} could be reached when operating at boundary flux conditions, as opposed to critical flux conditions.

2.2.3 Mathematical modelling in forward osmosis

The pore hindrance transport model was initially developed for neutral solutes in pressure-driven nanofiltration [132]. Recently, Xie et al. applied the pore hindrance transport model for the first time to forward osmosis, to describe the rejection of trace organic contaminants (TrOCs) as a function of permeate water flux. The pore hindrance transport model relies on the steric hindrance to the entrance of a molecule into the pore as well as viscous resistance inside the pore [133]. In this model, the membrane is considered a bundle of cylindrical tubes of the same radius through which spherical solute particles enter randomly. The ratio of solute radius to the membrane pore radius is related by the distribution coefficient when steric interactions are considered. The size of uncharged solutes and permeation experiments are used to obtain retention and/or reflection coefficients which are then used to determine the average membrane pore radius and the ratio of solute radius to pore radius, $\lambda = \frac{r_s}{r_p}$. Another method to determine λ is from the Hagen-Poiseuille equation, in which experimental values of pure water permeability and the average pore radius obtained by steric hindrance pore model are input. Silva et al. compared several correlations from literature for the pore hindrance model and found that the most suitable correlation had been

proposed by Bungay and Brenner (Figure 28) [134], who provided a complete correlation for $0 < \lambda \leq 1$ [135].

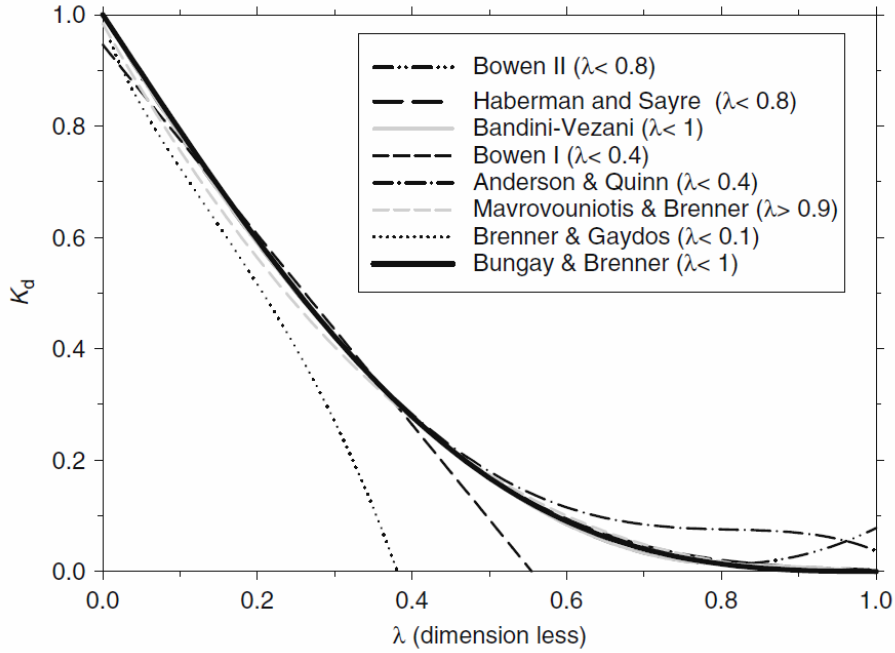

Figure 29: Diffusive pore hindrance factors from literature as a function of λ [134]

For both cellulose acetate and TFC polyamide membranes, the rejection of charged TrOCs was higher as they are rejected by both size exclusion and electrostatic repulsion (Figure 29). For neutral TrOCs, rejection was greater through the TFC membranes although they have the larger pore size, which the authors attributed to greater pore hydration. Pore hydration is the attachment of a layer of water molecules to the negatively charged membrane surface via hydrogen bonding. Greater pore hydration results in reduced effective membrane pore size which translates to enhanced steric hindrance and separation during the FO process.

Phuntsho et al. used established mass transport models to simulate a plate-and-frame FO membrane module [136]. They studied the effect of various operating parameters on water flux, feed recovery rate, and the final concentration of the diluted draw solution. They found that the counter-current crossflow mode of operation leads to greater water flux, higher recovery, as well

as higher DS final concentration, all of which are indicative of improved performance. From their analysis, they developed a modified equation for the water extraction capacity of a draw solute, which can form the basis of optimization studies on large-scale FO operations.

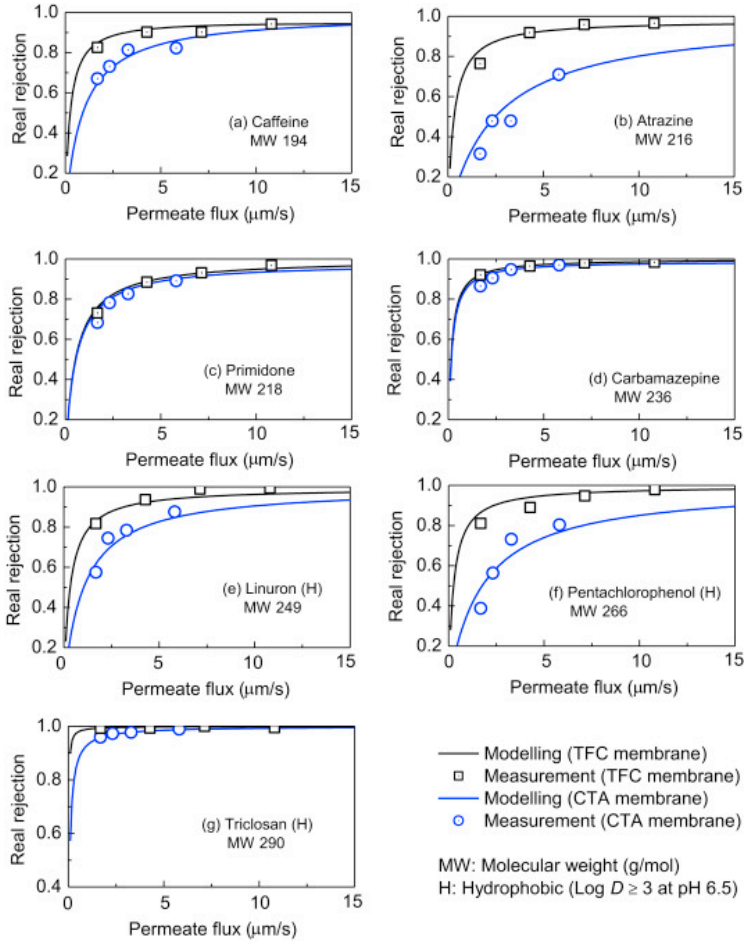

Figure 30: Real rejection of neutral TrOCs vs. permeate water flux by TFC and CTA membranes; solid lines represent predictions from the membrane pore hindrance transport model [137]

Lee et al. developed a characterization method for FO membranes by combining a statistical approach with a single experimental FO test [138]. The experimental component was carried out to measure the water and reverse solute flux in the feed solution where DI water was used as the feed and NaCl as the draw solute. They used a statistical approach to find the optimal water

permeability, salt permeability and resistance to salt diffusion in the support layer to predict the water and reverse solute flux using ICP and ECP models [138]. Results from the model were in close agreement with experimental values and can be used to predict experimental water and reverse solute flux.

Attarde et al. also used the ECP and ICP models and combined them with the Spiegler-Kedem model to also allow description of mass transport through the active layer of a spiral wound FO module [139]. They applied a nonlinear constrained optimization technique, together with experimental FO data, to predict the unknown parameters and minimize the error function. To minimize the error function, they used a hybrid function technique which includes a genetic algorithm technique and Fmincon from MATLAB. First, the genetic algorithm reaches the region close to the optimum point and uses that point as the initialization point for the Fmincon [139]. Figure 30 shows the simple algorithm used by Attarde et al. to determine unknown model parameters. Comparing the SK model with the traditional solution diffusion model, they found that the FO performance predicted in terms of permeate flux, solute flux as well as power density differed between the two models.

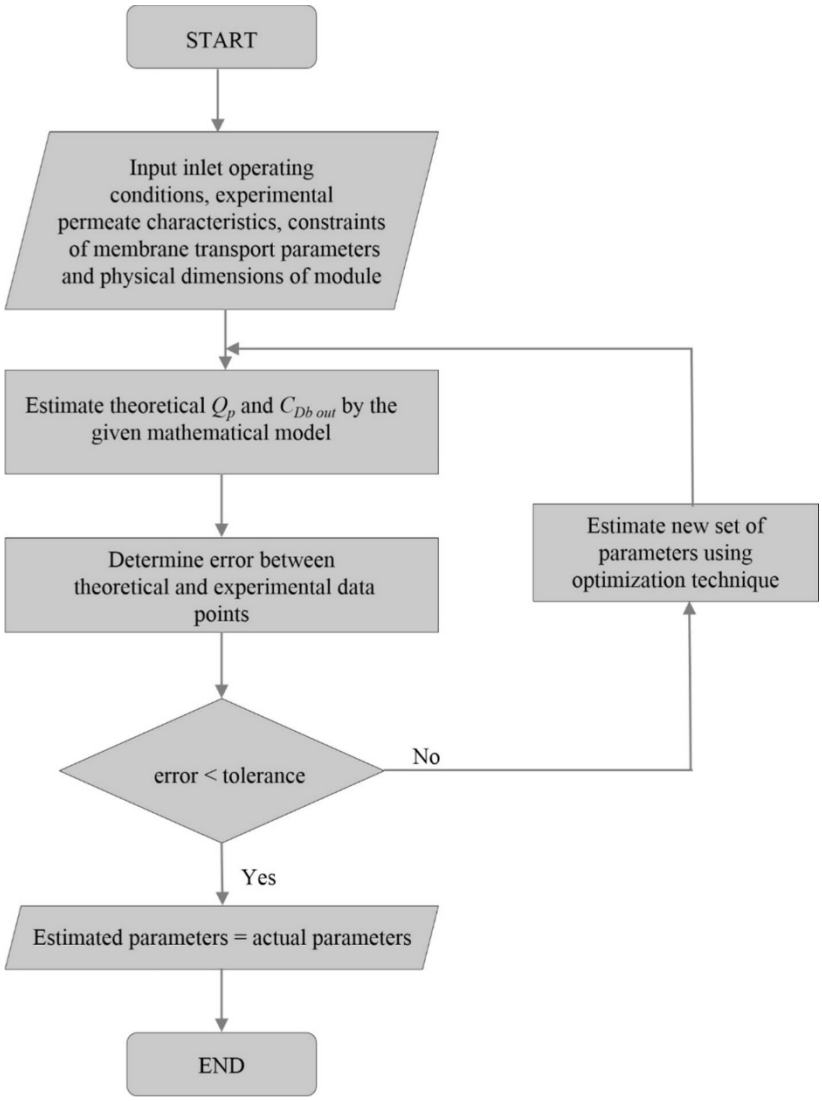

Figure 31: Algorithm for estimation of unknown model parameters; Q_p and $C_{Db,out}$ are the permeate flow rate and bulk draw solution concentration [139]

In FO, permeation of the draw solute through the membrane in reverse lowers the driving force for water flux, adversely affects the feedwater quality, and is also met with resistance from the foulant cake layer on the membrane surface. The foulant layer increases CP and cake-enhanced osmotic pressure (CEOP) and reduces water flux. Modelling can help overcome limitations of experimental instruments to study the various aspects of fouling in FO, allowing researchers to evaluate the effect of changing physical and chemical parameters on FO fouling without an experimental setup. Given the potential of modelling in this area, and the rapid growth of research

in FO, the limited number of studies carried out to investigate fouling in FO processes is startling. Park et al. developed a numerical model to predict the flux decline due to colloidal fouling in an FO membrane system [107]. They used a control volume approach and assumed that the cake layer growth is based on a first-order reaction to derive the kinetic equation; see the schematic shown in Figure 31. They found that the resistance of the cake layer is a major contributor to flux decline in the beginning, but increased reverse draw solute permeation through the membrane had little effect on flux decline. However, flux decline depends on the diffusivity, and hence the selection of the draw solute used in the process.

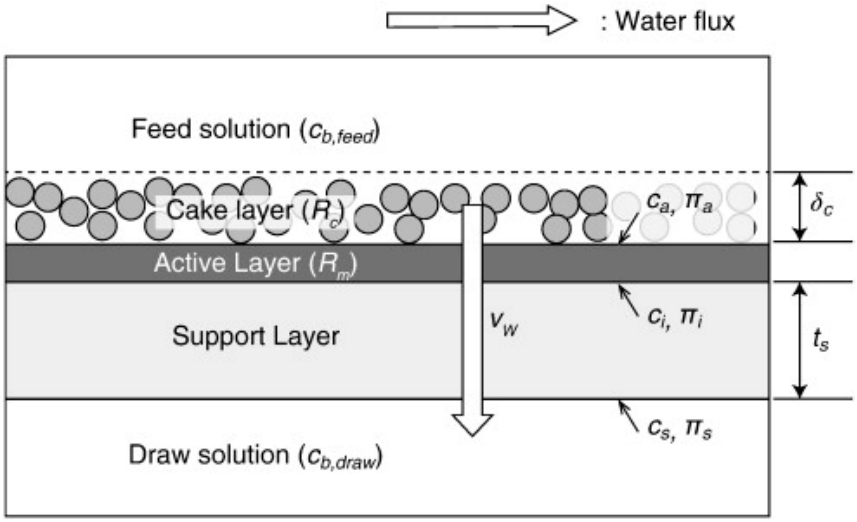

Figure 32: Schematic of simulated FO system with cakelike fouling [107]

They used the resistance-in-series model used to express the flux of an osmotically driven process as:

$$J_w = \frac{\Delta\pi}{\mu R} = \frac{\pi_i - \pi_a}{\mu(R_m + R_c)}$$

J_w is the permeate flux; π_i and π_a are the osmotic pressures of the active layer-support layer interface and active layer surface, respectively; μ is the dynamic viscosity; R, R_m and R_c refer to the membrane resistance, intrinsic membrane resistance, and cake layer resistance, respectively.

Recently, Wang et al. modified the solution-diffusion model to incorporate draw solution concentration and operating temperature and focused on maximizing FO water flux with respect to these parameters for a commercial thin-film composite membrane [140]. They quantified the effect of each parameter using a concentration-induced flux increment (CIE) and a temperature-induced flux increment efficiency (TIE). Interestingly, CIE increased with an increase of draw solution concentration and increased with an increase in temperature. On the other hand, the TIE increased when the temperature was raised from 25 to 47 °C and also increased for increased draw solution strength. Figure 32 shows that values projected theoretically were aligned with those obtained experimentally for a range of draw solution concentrations at different temperatures [140]. Through this study, they identified temperature-sensitive and concentration-sensitive regions (Figure 33), which can be of significance for optimizing FO water flux.

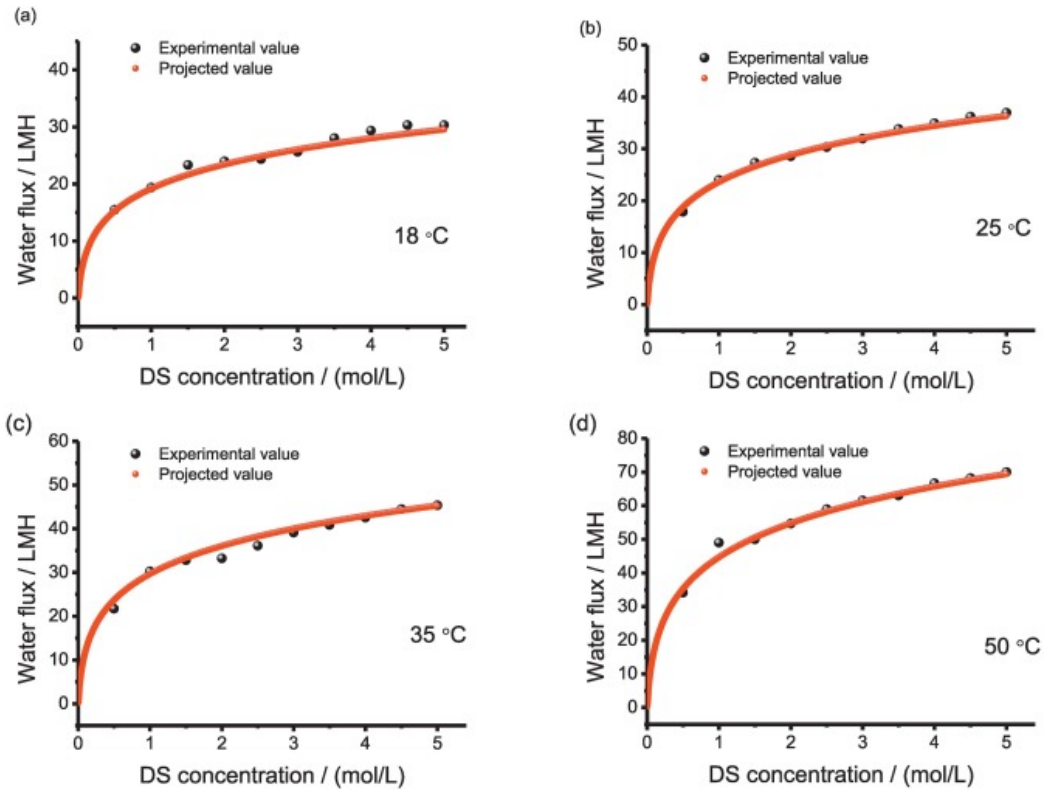

Figure 33: Predicted and experimental values of water flux vs. draw solution concentration at different temperatures [140]

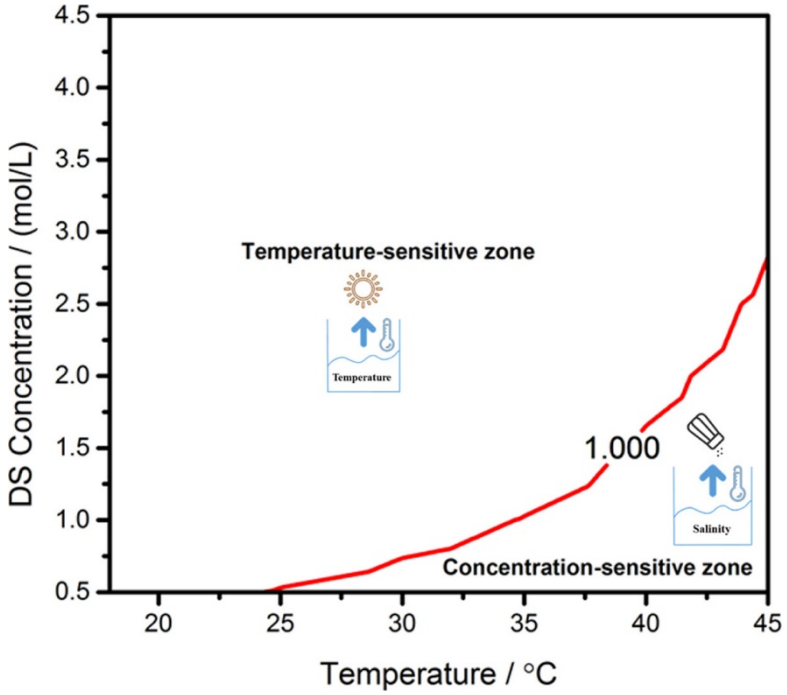

Figure 34: Temperature and draw solution concentration-sensitive zone as determined by Wang et al.'s modified solution

diffusion model. Red line indicates where water flux is equally sensitive to temperature and concentration [140]

Modelling approaches for FO fouling hold strong potential for growth and development of such techniques will help not only in predicting fouling in FO, but also in optimizing operational parameters for high rejection, high flux FO.

Table 7 shows process parameters and intrinsic membrane properties that can be optimized for selected membrane processes according to developed models.

Table 7: Selected variables and objective functions for membrane-based desalination processes [116, 119, 140]

Process	Objective function	Variables	Models used
Reverse osmosis	Maximize performance index	• Increase feed temperature • Increase operating pressure (Effects more significant at lower salt concentration)	RSM, ANN
Nanofiltration	Maximize multivalent ion rejection for low pressure softening	• Increase Pore dielectric constant • Decrease ore size • Not very sensitive to membrane charge density and membrane thickness	DSPM-DE
Forward osmosis	Maximize water flux	• Increase draw solution concentration • Increase operating temperature	Modified solution-diffusion model

2.3 Modelling of hybrid desalination technologies

Filippini et al. analyzed a hybrid MED and RO system for seawater desalination by developing

models for each of the two systems and an integrated model to evaluate several configurations of the two processes in the hybrid system [141]. Y. Chan modelled mass transport through nanomaterials, in particular carbon nanotubes and graphene sheets, as membrane materials for RO [142]. Shahzad et al. [143] proposed a tri-hybrid system consisting of RO and a multi-evaporator adsorption system (ME-AD), arranged in series for maximum recovery from pretreated feed. Theoretical results show that the overall recovery rate for seawater desalination on this hybrid system can be as high as 81%. Coupling of RO with thermal desalination systems as well as with renewable energy systems has been briefly reviewed by Qasim et al. [144] in a recent review.

Pretreatment is usually carried out to reduce the natural organic matter and suspended solids in the feed to minimize fouling in the desalination unit. However, most pretreatment processes do not involve removal of dissolved solids such as multivalent ions that can later precipitate and cause scaling on heat exchangers, which reduces the heat transfer efficiency in both MSF and MED systems [145]. Although antiscalants are used to prevent scaling, pretreatment needs to be able to remove multivalent ions. Nanofiltration and forward osmosis have been considered as pretreatment alternatives for MSF and MED. Due to nanofiltration being an energy-intensive pressure-driven process, a few recent studies have investigated the application of FO as pretreatment to thermal desalination. Thabit et al. experimentally optimized FO operating conditions for pretreatment to MSF and found that increasing the brine temperature from 25 °C to 40 °C leads to a flux increase of 32%.

As pressure-driven processes rely on hydraulic pressure from high-pressure pumps, forward osmosis (FO) offers a low-energy alternative. FO depends on the osmotic pressure difference between a concentrated draw solution and a feed stream across a semi-permeable membrane [146]. Apart from draw solute recovery and internal concentration polarization, FO membranes are still

susceptible to fouling, although to a lesser degree than membranes in hydraulic pressure-driven processes such as RO [107]. Fouling in FO has been found to be more reversible and less compacted as compared to RO [147]. Altaee and Zaragoza have developed a model to estimate power consumption in FO for seawater softening in an FO-MSF plant [148, 149]. Figure 35 shows the steps used to predict the concentration of diluted draw solution and estimated permeate flow for each recovery rate.

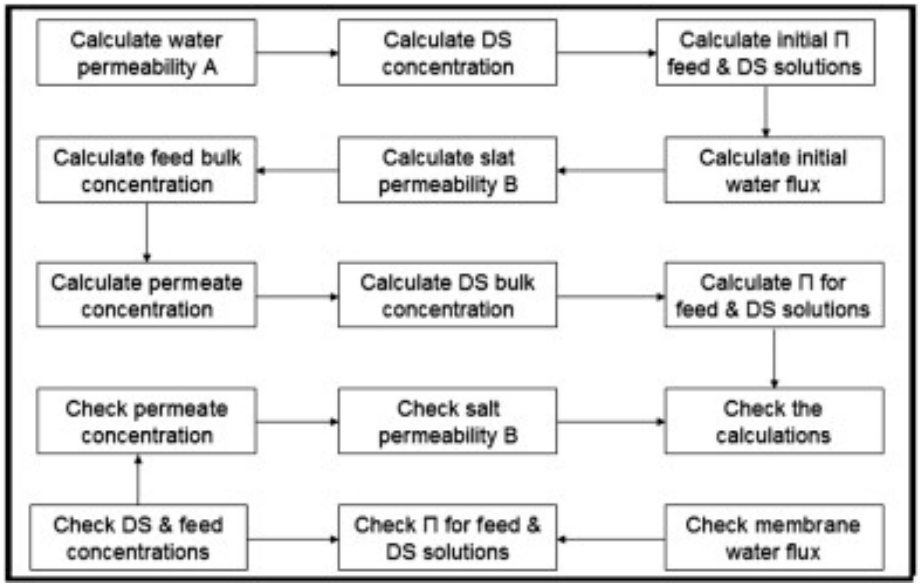

Figure 35: Procedure to estimate FO membrane performance [149]

Comparing the water flux and power consumption in FO to that in NF for pretreatment of MSF, Altaee and Zaragoza found that although water flux in NF is higher than in FO, specific power consumption and, hence, operation cost is higher for NF than for FO. However, feed salinity did not affect the power consumption in FO whereas power consumption for NF increased with salinity. In another study, Altaee et al. applied the same model to evaluate the effectiveness of FO pretreatment in the removal of divalent ions for a high temperature FO-MSF/MED hybrid system [150]. They simulated MSF at 130 °C using FO as pretreatment and calculated the concentration of Ca^{2+} and SO_4^{2-} ions in each stage. They found that FO pretreatment increased MED TBT to 85

°C, which led to a distillate flow rate 1.8 times higher than a TBT of 65 °C. They also developed an FO pretreatment-MED Scale Index (FMSI) to determine the required FO recovery rate to avoid scale problems. This scale index was based on calculating the Ryznar Scale Index (RSI) with different MED operating temperatures and FO recovery rates. They then used the FMSI to determine the required mixing ratio for FO and NF feed as a pretreatment for MED and found that FO pretreatment is more efficient than NF for scale removal.

Pal et al. recently modelled an integrated FO-NF system for the treatment of hazardous wastewater [151]. They applied a flat sheet cross flow FO membrane module coupled with an NF system to recover the draw solute. The developed model is based on solution-diffusion mechanism for FO while the DSPM with dielectric exclusion phenomenon is used to describe the NF component. The transport mechanisms that dominate NF are diffusion, convection, and electromigration while only the latter two exist in the case of FO. As mentioned earlier, ionic separation at the solution-membrane interface is described by Donnan equilibrium and steric effects. Dielectric exclusion phenomenon is included because DSPM on its own is suitable for uncharged solutes, but not in the case of mixed electrolytes solution and/or multivalent ions [152]. They found that performance predicted by the model was in agreement with experimental data with a low relative error of < 0.1 and a high correlation coefficient; these results suggested that their model will help scale-up of this hybrid system. Zaviska and Zou modelled a bench scale FO process as pretreatment for RO and found that FO can help avoid RO fouling while achieving higher permeate recovery [153]. In this simulation, the diluted draw solution becomes the RO feed and is then re-concentrated for reuse in FO. The model took into account flux, water recovery, and the final draw solution. They assumed 1000 m^3/day of RO feed (i.e., diluted draw solution outlet from FO process) which is treated using 1000 m^2 RO membrane, together with a pressure exchanger as ERD. They used their

model to determine the operating pressure and energy consumption required for RO.

Senthil and Senthilmurugan simulated an integrated SWRO-PRO system for eliminating post-treatment of brine from RO. By modelling six SWRO-PRO configurations using seawater as feed solution, they found that direct mixing of diluted PRO draw solution with RO feed could reduce SEC by 49%, in comparison to SWRO alone [154].

Obaidi et al. [155] analyzed a multistage multi-pass medium-sized brackish water RO (BWRO) desalination plant in Jordan, producing 1200 m^3/day. For the spiral wound RO membranes, they developed a model based on solution diffusion and employed it to simulate operation of low-salinity BWRO. Plant data obtained experimentally was in line with results from the simulation, as shown in Figure 36. When they carried out sensitivity analysis on their model, they found that feed flow rate and operating pressure are the main factors affecting product salinity.

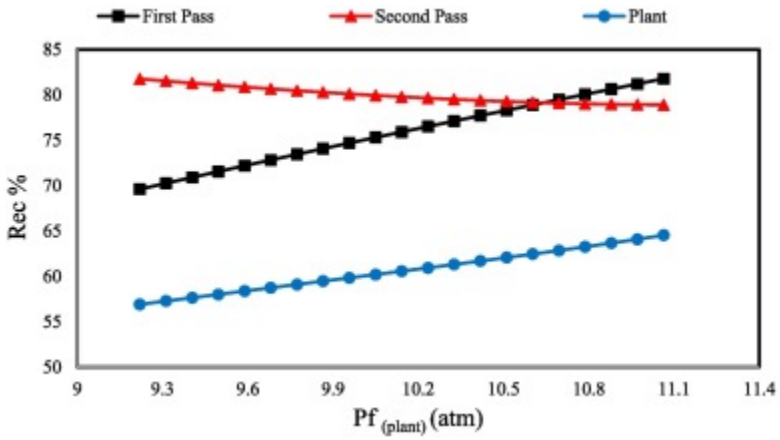

Figure 36: Effect of plant operating pressure on recovery rate of pass 1, pass 2, and total [155]

Malik *et al.* optimized MSF, RO and MSF-RO desalination systems for a total production capacity of 89,394 m3/day [156]. They developed a superstructure to analyze various configurations of RO alone, MSF alone and RO/MSF hybrid and additional equipment such as mixers and splitters, to allow analysis on a single flowsheet (Figure 37). Using a feed separator eliminates the need for multiple flowsheets. They optimized operating and design variables and found that the hybrid

system has a higher overall recovery and lower operating cost than the MSF system and better product water quality than RO alone.

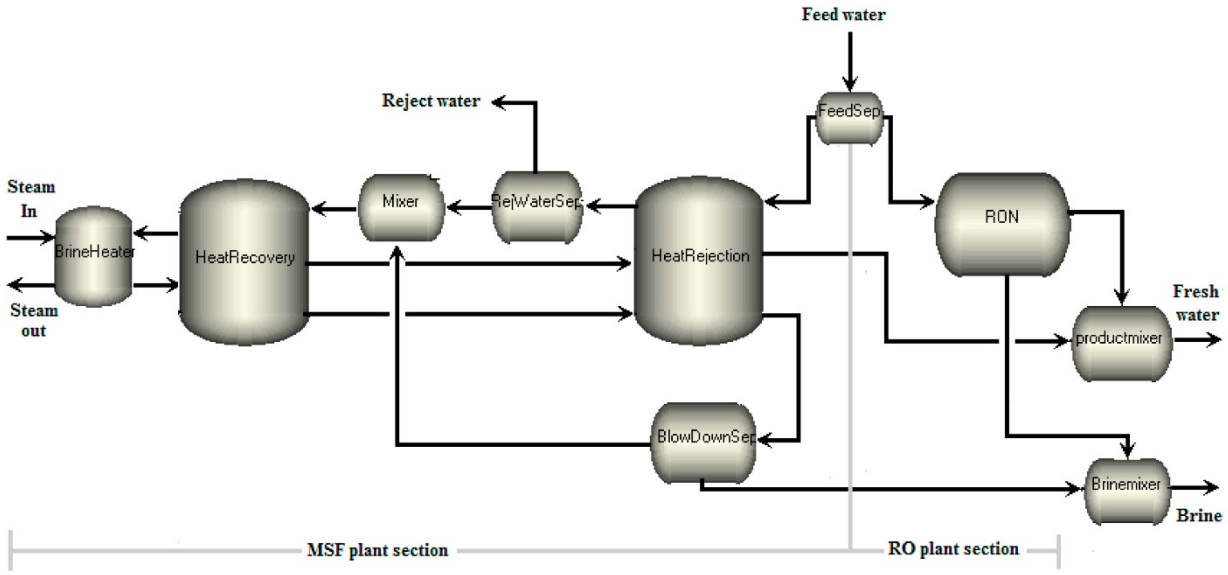

Figure 37: Desalination superstructure schematic used to analyze various MSF/RO configurations [156]

Bartholomew [157] developed a cost optimization model for osmotically assisted RO, in which they investigated the relationship between membrane stages, saline sweep cycles, and makeup, purge and recycle streams for high-salinity feeds in the range of 50,000 to 125,000 ppm TDS. The optimized design resulted in costs less than $\$6/m^3$ water with water recoveries between 30-70%. They studied 3 cases: (1) feed TDS of 75 g/L and 50% water recovery, (2) feed TDS of 75 g/L and 70% water recovery, and (3) feed TDS of 125 g/L and 40% water recovery [157]. They found that cost-optimal unit water cost was the lowest for case 1, as shown in Figure 38A. Figure 38B shows the normalized costs of the various components (membrane capital and replacement costs, capital costs of pumps, pressure exchanger, electricity costs and other operating expenses). They used a nonlinear optimization model with the objective of minimizing the cost of the OARO system and found that OARO can be economically feasible for feed salinities of up to 125 g/L and water recoveries of up to 70% [157].

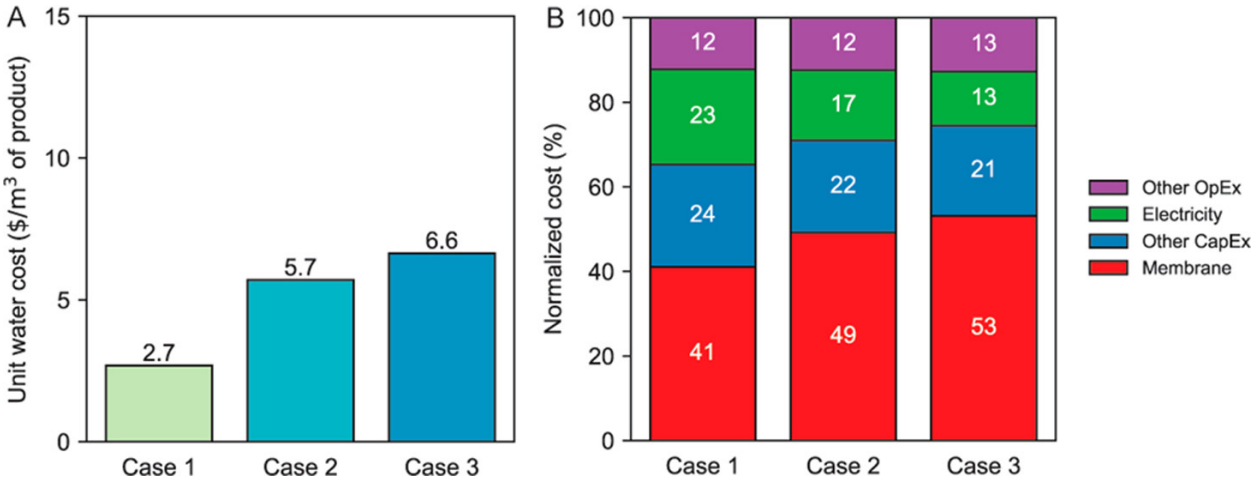

Figure 38: Cost-optimal unit water costs (A) and normalized component costs (B) for the three cases studied by for OARO of high-salinity brine [157]

3. Future direction

3.1 Modelling of renewable energy systems with desalination

Despite reduced energy consumption, energy still makes up the largest portion of overall costs in desalination systems. With comparable advances in renewable energy systems such as solar and wind energies [158], the use of renewable energy to power desalination is now being considered an important alternative for providing fresh water, as is evident from the large number of reviews on this topic [159-164]. Modelling the coupling of RE systems with desalination technologies is an active area of research with tremendous potential. Several studies have recently been carried out on the integration of renewable energy systems with desalination systems, including hybrid RE systems such as wind-geothermal, solar-wind, etc. [164-169]. Solar energy desalination is of particular interest and the most widely form of renewable coupled with desalination, as the most water scarce regions are also those with the greatest solar energy abundance [170]. Kasaeian et al. [171] recently reviewed desalination by solar energy, focusing on RO and FO technologies, in which they included several recent modelling and simulation studies. Often, each segment, the renewable energy system and the desalination system, is optimized separately [172].

Mentis et al. developed a multiparameter dimensioning tool to evaluate the integration of renewable energy with RO desalination on the islands of South Aegean Sea. The model includes different desalination capacities depending on the size and water demand of the island, selection of appropriate renewable energy technology for supplying electricity to the RO plant, energy balances of the integrated system, and the cost of water production and electricity [173]. They found that the price of water on the smaller island would be greater; however, RE would enable both islands to sell water at a much lower cost than the current price.

Salehi et al. investigated the feasibility of producing distilled water with a geothermal power system [174]. They applied a three-objective optimization procedure on a geothermal power plant using a genetic algorithm, focused on optimizing electricity output, product unit cost, and distilled water flowrate. In their study, which consisted of a double-flash geothermal power plant, the decision parameters were the pressures of the two flash chambers and the temperatures of the vaporator and generator. They compared two configurations of integrating a geothermal power system with thermal distillation: one in which the reinjected geofluid temperature is assumed to have a temperature of above 100 °C, and another in which the temperature is below 100 °C, but is enhanced with an absorption heat transformer and the upgraded thermal energy is used to produce purified water. They found that the first configuration yielded higher distilled water flow rates,but the second configuration resulted in higher power outputs.

Heidary *et al.* [175] recently designed a small scale MSF-RO desalination system producing 25 liters per hour and powered by hybridization of solar and wind. For the desalination system, they studied six models and optimized air pressure, seawater temperature, seawater flow rate and seawater salinity to minimize water production costs and maximize the volume of product water. Figure 28 shows a schematic of the hybrid solar wind MSF-RO system. For the hybrid solar wind

energy system, they proposed an energy system composed of wind turbine, solar panel and solar collector, electricity from all of which is saved in batteries. In the mathematical model, the weather conditions, design parameters of the RO-MSF models and the energy demand of the desalination system were considered input variables.

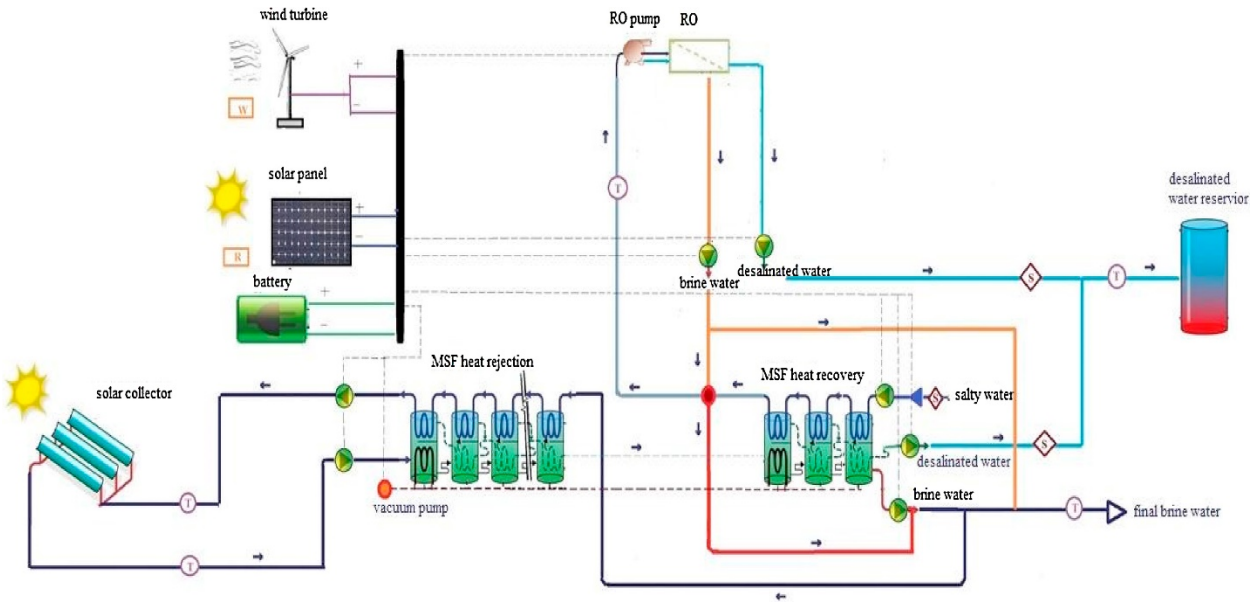

Figure 39: Schematic of hybrid solar-wind MSF-RO desalination system

The greatest water production was obtained with an integrated MSF-RO system, where part of the brine from MSF goes through a single pass RO while the remaining is mixed with RO brine. The system where the heat rejection of the MSF condenser liquid is used as feed for the RO was shown to be the most energy efficient for large-scale production of > 1000 L/hour.

The cost of the hybrid system is the sum of the total cost for each subsystem i.e. wind, solar, battery, RO and MSF system, which includes direct and indirect capital costs as well as operation and maintenance costs. Economic optimization based on maximizing water production and minimizing water cost for each of the configurations showed that hybridization of wind-solar and RO-MSF were the optimal choices when compared to fossil fuel RO or MSF, fossil fuel RO-MSF, wind RO, wind MSF, solar RO or solar MSF alone.

3.2 Other challenges

Future direction involves lowering the energy consumption of newer membrane-based processes such as FO through novel process design and configuration optimization, as has been the case for RO recently. Among renewable energy systems for desalination, most of the modelling has focused on photovoltaics coupled with reverse osmosis. More studies need to be carried out to study the coupling of other desalination processes as well as hybrid RE systems. Additionally, research in integration of new generation artificial intelligence algorithms into desalination is still in its infancy and is expected to grow in coming years. As mentioned earlier, modelling and experimental studies go hand in hand, and for many of the more complex or newer processes such as nanofiltration, measuring tools are still lacking in providing a complete understanding of the process. To design models that will reflect performance closer to real systems, concurrent advancements in measurement methods and tools are necessary. Additionally, the same complex processes may require hybridization of conventional and artificial intelligence models – an area in which very limited work has been carried out to date. As has been shown in some of the studies highlighted in this review, nondeterministic algorithms are becoming more relevant due to their ability to model systems for a wider range of operating conditions that is not often possible with conventional methods. Research will focus on benefitting from the strengths of the two types of approaches, integrating them to achieve accurate solutions for complex systems using the least amount of resources. Another area of particular interest is the model-based process control in membrane-based technology.

4. Conclusion

As installed desalination capacity grows worldwide, there is an imminent need to reduce energy

consumption for desalination processes either through new configurations and process design for existing processes, development of new technologies, and/or through optimization of operational parameters. Each of these solutions necessitates the need for model building to accurately describe and analyze desalination processes. In the area of thermal desalination, although some new configurations have been studied through modelling, the technology is reaching saturation and recent studies are focused on understanding and controlling scale behavior on surfaces. For the duration thermal desalination has been around, it is surprising that scale formation affecting MSF performance was very little understood before recent years. For RO, modelling tools are being used to assess the feasibility of new configurations of the membrane module, with much attention on internally staged design modules to balance flux through the module and, hence, to minimize energy consumption. For other pressure-driven membrane processes such as nanofiltration, simple models are being modified to develop a deeper understanding of the transport mechanism, which takes into account diffusion and convection through the pores and/or charged membrane.

Regarding the aspects discussed in this literature survey, there are a few gaps in literature we have identified that could direct further research in this field.

- The use of artificial intelligence models to control desalination processes offers a promising avenue of exploration.
- Experimental studies in optimization of membrane materials and draw solutions for FO are still needed before modelling novel system configurations.
- In continuation of the above point, although mathematical models membrane processes continue to be developed, resulting optimization of intrinsic membrane properties through modelling is still limited in comparison to modelling of operating conditions and other process properties, especially for newer processes.

- Modelling new FO membrane and module configurations could be useful in using FO as a pretreatment technology for MSF or RO, either separately or in hybrid with other desalination processes. Currently, the diluted draw solution needs to be further treated and studies of such hybrid FO systems are still limited. This step would help determine the feasibility of employing FO in large-scale desalination.
- The use of models to predict specific kinds of fouling for all membrane-based desalination processes, including newer processes such as forward osmosis and membrane distillation, could open a whole new avenue for research. This means more models for validating the fouling behavior of membrane surfaces need to be developed.

5. References

1. *Global Desalination Market 2018-2022: Rising Popularity of Forward Osmosis, Nanofiltration, and Other High-Performance Membrane-Based Technologies*. 2018, M2PressWIRE.
2. Gude, V.G., *Desalination and water reuse to address global water scarcity.* Reviews in Environmental Science and Bio/Technology, 2017. **16**(4): p. 591-609.
3. El-Dessouky, H.T. and H.M. Ettouney, *Chapter 1 - Introduction*, in *Fundamentals of Salt Water Desalination*, H.T. El-Dessouky and H.M. Ettouney, Editors. 2002, Elsevier Science B.V.: Amsterdam. p. 1-17.
4. Bremere, I., et al., *How water scarcity will effect the growth in the desalination market in the coming 25 years.* Desalination, 2001. **138**(1): p. 7-15.
5. Caldera, U. and C. Breyer, *Learning Curve for Seawater Reverse Osmosis Desalination Plants: Capital Cost Trend of the Past, Present, and Future.* Water Resources Research, 2017. **53**(12): p. 10523-10538.
6. Jones, E., et al., *The state of desalination and brine production: A global outlook.* Science of The Total Environment, 2019. **657**: p. 1343-1356.
7. Mayor, B., *Growth patterns in mature desalination technologies and analogies with the energy field.* Desalination, 2019. **457**: p. 75-84.
8. Roy, Y., et al., *The effect of increased top brine temperature on the performance and design of OT-MSF using a case study.* Desalination, 2017. **412**: p. 32-38.
9. Ghiazza, E., R. Borsani, and F. Alt, *Innovation in multistage flash evaporator design for reduced energy consumption and low installation cost.* Int. Desalin. Assoc. World Congr. Desalin. Water Reuse/Tianjin, China, 2013.
10. Tonner, J.B., S. Hinge, and C. Legorreta, *Plates—the next breakthrough in thermal desalination.* Desalination, 2001. **134**(1-3): p. 205-211.
11. El-Halwagi, M.M., *Sustainable Design Through Process Integration: Fundamentals and*

Applications to Industrial Pollution Prevention, Resource Conservation, and Profitability Enhancement. 2017: Elsevier Science.
12. Ettouney, H., *Conventional Thermal Processes*, in *Seawater Desalination: Conventional and Renewable Energy Processes*, G. Micale, L. Rizzuti, and A. Cipollina, Editors. 2009, Springer Berlin Heidelberg: Berlin, Heidelberg. p. 17-40.
13. Gebel, J., *Thermal Desalination Processes*, in *Desalination*. p. 51-138.
14. Omar, A.M., *Simulation of M.S.F. desalination plants.* Desalination, 1983. **45**(2): p. 65-76.
15. Helal, A.M., et al., *Optimal design of hybrid RO/MSF desalination plants Part I: Modeling and algorithms.* Desalination, 2003. **154**(1): p. 43-66.
16. Rosso, M., et al., *Modeling multistage flash desalination plants.* Desalination, 1997. **108**(1): p. 365-374.
17. Lalia, B.S., et al., *A review on membrane fabrication: Structure, properties and performance relationship.* Desalination, 2013. **326**: p. 77-95.
18. Ismail, A.F., K.C. Khulbe, and T. Matsuura, *Chapter 1 - Introduction—Do RO Membranes Have Pores?*, in *Reverse Osmosis*, A.F. Ismail, K.C. Khulbe, and T. Matsuura, Editors. 2019, Elsevier. p. 1-24.
19. El-Dessouky, H.T., H.M. Ettouney, and H.M. Ettouney, *Fundamentals of Salt Water Desalination*. 2002, Oxford, NETHERLANDS, THE: Elsevier Science & Technology.
20. Belfort, G., *Synthetic Membrane Process : Fundamentals and Water Applications*. 1984, Saint Louis, UNITED STATES: Elsevier Science & Technology.
21. Wang, J., et al., *A critical review of transport through osmotic membranes.* Journal of Membrane Science, 2014. **454**: p. 516-537.
22. Gao, W., et al., *Understanding water and ion transport behaviour and permeability through poly(amide) thin film composite membrane.* Journal of Membrane Science, 2015. **487**: p. 32-39.
23. Jiang, S., Y. Li, and B.P. Ladewig, *A review of reverse osmosis membrane fouling and control strategies.* Science of The Total Environment, 2017. **595**: p. 567-583.
24. Wenten, I.G. and Khoiruddin, *Reverse osmosis applications: Prospect and challenges.* Desalination, 2016. **391**: p. 112-125.
25. Sidney, L. and S. Srinivasa, *High flow porous membranes for separating water from saline solutions*. 1964, Google Patents.
26. Lin, S. and M. Elimelech, *Staged reverse osmosis operation: Configurations, energy efficiency, and application potential.* Desalination, 2015. **366**: p. 9-14.
27. Bowen, W.R. and A.W. Mohammad, *Characterization and Prediction of Nanofiltration Membrane Performance—A General Assessment.* Chemical Engineering Research and Design, 1998. **76**(8): p. 885-893.
28. Agboola, O., et al., *Theoretical performance of nanofiltration membranes for wastewater treatment.* Environmental chemistry letters, 2015. **13**(1): p. 37-47.
29. Wang, L.K., et al., *Membrane and Desalination Technologies*. 2010: Humana Press.
30. Jye, L.W. and A.F. Ismail, *Nanofiltration Membranes : Synthesis, Characterization, and Applications*. 2016, Boca Raton, UNITED KINGDOM: CRC Press LLC.
31. Linares, R.V., et al., *Recent Developments in Forward Osmosis Processes*. 2017, London, UNITED KINGDOM: IWA Publishing.
32. Cath, T.Y., A.E. Childress, and M. Elimelech, *Forward osmosis: Principles, applications, and recent developments.* Journal of Membrane Science, 2006. **281**(1): p. 70-87.
33. Yahaya, N.Z.S., et al., *Chapter 10 - Forward Osmosis for Desalination Application*, in

Membrane Separation Principles and Applications, A.F. Ismail, et al., Editors. 2019, Elsevier. p. 315-337.
34. Greenlee, L.F., et al., *Reverse osmosis desalination: water sources, technology, and today's challenges.* Water research, 2009. **43**(9): p. 2317-2348.
35. Guo, W., H.-H. Ngo, and J. Li, *A mini-review on membrane fouling.* Bioresource Technology, 2012. **122**: p. 27-34.
36. Burn, S. and S. Gray, *Efficient Desalination by Reverse Osmosis : A guide to RO practice*. 2015, London, UNITED KINGDOM: IWA Publishing.
37. Wang, K.Y., R.C. Ong, and T.-S. Chung, *Double-skinned forward osmosis membranes for reducing internal concentration polarization within the porous sublayer.* Industrial & Engineering Chemistry Research, 2010. **49**(10): p. 4824-4831.
38. Gray, G.T., J.R. McCutcheon, and M. Elimelech, *Internal concentration polarization in forward osmosis: role of membrane orientation.* Desalination, 2006. **197**(1): p. 1-8.
39. Ersoy, Y. and A.O. Moscardini, *Mathematical Modelling Courses for Engineering Education*. 2013: Springer Berlin Heidelberg.
40. Sarker, R.A. and C.S. Newton, *Optimization modelling: a practical approach*. 2007: CRC press.
41. Barth, T.J., M. Griebel, and D.E. Keyes, *Multiscale Modelling and Simulation*. 2002, Berlin/Heidelberg, GERMANY: Springer Berlin Heidelberg.
42. Cross, M. *The Role and Practice of Mathematical Modelling in Industry Today*. in *Mathematical Modelling Courses for Engineering Education*. 1994. Berlin, Heidelberg: Springer Berlin Heidelberg.
43. Walker, D., et al., *Engineering Modelling and Analysis*. 2018: CRC Press.
44. Yang, X.-S. and S. Koziel, *Computational optimization and applications in engineering and industry*. Vol. 359. 2011: Springer Science & Business Media.
45. Van der Bruggen, B., *Chapter 2 - Microfiltration, ultrafiltration, nanofiltration, reverse osmosis, and forward osmosis*, in *Fundamental Modelling of Membrane Systems*, P. Luis, Editor. 2018, Elsevier. p. 25-70.
46. Sobana, S. and R.C. Panda, *Review on modelling and control of desalination system using reverse osmosis.* Reviews in Environmental Science & Biotechnology, 2011. **10**(2): p. 139-150.
47. Blanco-Marigorta, A.M., A. Lozano-Medina, and J.D. Marcos, *A critical review of definitions for exergetic efficiency in reverse osmosis desalination plants.* Energy, 2017. **137**: p. 752-760.
48. Qasim, M., et al., *Water desalination by forward (direct) osmosis phenomenon: A comprehensive review.* Desalination, 2015. **374**: p. 47-69.
49. Shang, W., D. Wang, and X. Wang, *Modeling of the separation performance of nanofiltration membranes and its role in the applications of nanofiltration technology in product separation processes.* Frontiers of Chemical Engineering in China, 2007. **1**(2): p. 208-215.
50. Oatley-Radcliffe, D.L., et al., *Critical appraisal of current nanofiltration modelling strategies for seawater desalination and further insights on dielectric exclusion.* Desalination, 2014. **343**: p. 154-161.
51. Yaroshchuk, A., M.L. Bruening, and E. Zholkovskiy, *Modelling nanofiltration of electrolyte solutions.* Advances in Colloid and Interface Science, 2019. **268**: p. 39-63.
52. Oatley-Radcliffe, D.L., et al., *Nanofiltration membranes and processes: A review of*

research trends over the past decade. Journal of Water Process Engineering, 2017. **19**: p. 164-171.
53. Al Aani, S., et al., *Can machine language and artificial intelligence revolutionize process automation for water treatment and desalination?* Desalination, 2019. **458**: p. 84-96.
54. Mahadevaa, R., et al., *Modelling and simulation of desalination process using artificial neural network: a review.* DESALINATION AND WATER TREATMENT, 2018. **122**: p. 351-364.
55. Mabrouk, A.N.A., *Technoeconomic analysis of once through long tube MSF process for high capacity desalination plants.* Desalination, 2013. **317**: p. 84-94.
56. Alsadaie, S.M. and I.M. Mujtaba, *Dynamic modelling of Heat Exchanger fouling in multistage flash (MSF) desalination.* Desalination, 2017. **409**: p. 47-65.
57. Kern, D. and R. Seaton, *Surface fouling: how to calculate limits.* Chem. Eng. Prog, 1959. **55**(6): p. 71-73.
58. Cooper, K.G., et al., *A model for the fouling of M.S.F. plants based on data from operating units.* Desalination, 1983. **47**(1): p. 37-42.
59. Gazit, E. and D. Hasson, *Scale deposition from an evaporating falling film.* Desalination, 1975. **17**(3): p. 339-351.
60. Hasson, D., et al., *Mechanism of calcium carbonate scale deposition on heat-transfer surfaces.* Industrial & Engineering Chemistry Fundamentals, 1968. **7**(1): p. 59-65.
61. Hasson, D., H. Sherman, and M. Biton. *Prediction of calcium carbonate scaling rates*. in *Proceedings 6th International Symposium Fresh Water from the Sea*. 1978.
62. Taborek, J., *Predictive Methods for Fouling Behavior.* Chem. Eng. Prog. Chem. Eng. Prog., 1972. **68**(7): p. 69-78.
63. Müller-Steinhagen, H. and C. Branch, *Influence of thermal boundary conditions on calcium carbonate fouling in double pipe heat exchangers: Einfluß der thermischen Randbedingungen auf die Ablagerung von CaCO3 in Doppelrohrwärmeübertragern.* Chemical Engineering and Processing: Process Intensification, 1988. **24**(2): p. 65-73.
64. Brahim, F., W. Augustin, and M. Bohnet, *Numerical simulation of the fouling process.* International Journal of Thermal Sciences, 2003. **42**(3): p. 323-334.
65. Zhang, F., J. Xiao, and X.D. Chen, *Towards predictive modeling of crystallization fouling: A pseudo-dynamic approach.* Food and Bioproducts Processing, 2015. **93**: p. 188-196.
66. Bott, T.R., *Fouling of heat exchangers*. 1995, Amsterdam ; New York: Elsevier.
67. Ibrahim, H.A.-H., *Fouling in heat exchangers*, in *MATLAB-A Fundamental Tool for Scientific Computing and Engineering Applications-Volume 3*. 2012, IntechOpen.
68. Al-Rawajfeh, A.E., et al., *Scale formation model for high top brine temperature multi-stage flash (MSF) desalination plants.* Desalination, 2014. **350**: p. 53-60.
69. Al-Anezi, K. and N. Hilal, *Scale formation in desalination plants: effect of carbon dioxide solubility.* Desalination, 2007. **204**(1): p. 385-402.
70. Shams El Din, A.M., M.E. El-Dahshan, and R.A. Mohammed, *Inhibition of the thermal decomposition of HCO3− A novel approach to the problem of alkaline scale formation in seawater desalination plants.* Desalination, 2002. **142**(2): p. 151-159.
71. Al-Sofi, M.A.-K., *Fouling phenomena in multi stage flash (MSF) distillers.* Desalination, 1999. **126**(1): p. 61-76.
72. Shams El Din, A.M., M.E. El-Dahshan, and R.A. Mohammed, *Scale formation in flash chambers of high-temperature MSF distillers.* Desalination, 2005. **177**(1): p. 241-258.
73. Zhao, J., et al., *A review of heterogeneous nucleation of calcium carbonate and control*

strategies for scale formation in multi-stage flash (MSF) desalination plants. Desalination, 2018. **442**: p. 75-88.
74. Al-Rawajfeh, A.E., *Nanofiltration pretreatment as CO2 deaerator of desalination feed: CO2 release reduction in MSF distillers.* Desalination, 2016. **380**: p. 12-17.
75. Hamed, O.A., *Scale control in multistage flash (MSF) desalination plants - lessons learnt*. 2017. p. 19-25.
76. Mabrouk, A.N.A. and H.E.-b.S. Fath, *Techno-economic analysis of hybrid high performance MSF desalination plant with NF membrane.* Desalination and Water Treatment, 2013. **51**(4-6): p. 844-856.
77. Al-Rawajfeh, A.E., H.E.S. Fath, and A.A. Mabrouk, *Integrated Salts Precipitation and Nano-Filtration as Pretreatment of Multistage Flash Desalination System.* Heat Transfer Engineering, 2012. **33**(3): p. 272-279.
78. Al-Sofi, M.A.K., et al., *Nanofiltration as a means of achieving higher TBT of ≥ 120°C in MSF.* Desalination, 1998. **118**(1): p. 123-129.
79. Abdelkader, B.A., et al., *Development of graphene oxide-based membrane as a pretreatment for thermal seawater desalination.* Desalination, 2019. **465**: p. 13-24.
80. Hanshik, C., et al., *Improved productivity of the MSF (multi-stage flashing) desalination plant by increasing the TBT (top brine temperature).* Energy, 2016. **107**: p. 683-692.
81. Ali, M.B. and L. Kairouani, *Multi-objective optimization of operating parameters of a MSF-BR desalination plant using solver optimization tool of Matlab software.* Desalination, 2016. **381**: p. 71-83.
82. Dahdah, T.H. and A. Mitsos, *Structural optimization of seawater desalination: I. A flexible superstructure and novel MED–MSF configurations.* Desalination, 2014. **344**: p. 252-265.
83. Bandi, C.S., R. Uppaluri, and A. Kumar, *Global optimization of MSF seawater desalination processes.* Desalination, 2016. **394**: p. 30-43.
84. Mathai, A.M. and H.J. Haubold, *Non-deterministic Models and Optimization*, in *Fractional and Multivariable Calculus : Model Building and Optimization Problems*, A.M. Mathai and H.J. Haubold, Editors. 2017, Springer International Publishing: Cham. p. 107-181.
85. Glueckauf, E. *On the mechanism of osmotic desalting with porous membranes*. in *Proc. First Int. Conf. on Water Desalination*. 1965.
86. Oren, Y.S. and P.M. Biesheuvel, *Theory of ion and water transport in reverse osmosis membranes*. 2017.
87. Takeuchi, H., et al., *Emerging investigators series: a steric pore-flow model to predict the transport of small and uncharged solutes through a reverse osmosis membrane.* Environmental Science: Water Research & Technology, 2018. **4**(4): p. 493-504.
88. Ismail, A.F. and T. Matsuura, *Progress in transport theory and characterization method of Reverse Osmosis (RO) membrane in past fifty years.* Desalination, 2018. **434**: p. 2-11.
89. Hall, M.S., D.R. Lloyd, and V.M. Starov, *Reverse osmosis of multicomponent electrolyte solutions Part II. Experimental verification.* Journal of membrane science, 1997. **128**(1): p. 39-53.
90. Hall, M.S., V.M. Starov, and D.R. Lloyd, *Reverse osmosis of multicomponent electrolyte solutions Part I. Theoretical development.* Journal of membrane science, 1997. **128**(1): p. 23-37.
91. Starov, V.M. and N.V. Churaev, *Separation of electrolyte solutions by reverse osmosis.* Advances in Colloid and Interface Science, 1993. **43**(2): p. 145-167.

92. Shen, M., S. Keten, and R.M. Lueptow, *Dynamics of water and solute transport in polymeric reverse osmosis membranes via molecular dynamics simulations.* Journal of Membrane Science, 2016. **506**: p. 95-108.
93. Zarzo, D. and D. Prats, *Desalination and energy consumption. What can we expect in the near future?* Desalination, 2018. **427**: p. 1-9.
94. Kim, J. and S. Hong, *Optimizing seawater reverse osmosis with internally staged design to improve product water quality and energy efficiency.* Journal of Membrane Science, 2018. **568**: p. 76-86.
95. Mousa, K., A. Diabat, and H. Fath, *Optimal design of a hybrid solar-wind power to drive a small-size reverse osmosis desalination plant.* Desalination and Water Treatment, 2013. **51**(16-18): p. 3417-3427.
96. Shaffer, D.L., et al., *Seawater desalination for agriculture by integrated forward and reverse osmosis: Improved product water quality for potentially less energy.* Journal of Membrane Science, 2012. **415-416**: p. 1-8.
97. Geise, G.M., et al., *Water permeability and water/salt selectivity tradeoff in polymers for desalination.* Journal of Membrane Science, 2011. **369**(1-2): p. 130-138.
98. Lin, S. and M. Elimelech, *Kinetics and energetics trade-off in reverse osmosis desalination with different configurations.* Desalination, 2017. **401**: p. 42-52.
99. Jeong, K., M. Park, and T.H. Chong, *Numerical model-based analysis of energy-efficient reverse osmosis (EERO) process: Performance simulation and optimization.* Desalination, 2019. **453**: p. 10-21.
100. Chong, T.H. and W.B. Krantz, *Process economics and operating strategy for the energy-efficient reverse osmosis (EERO) process.* Desalination, 2018. **443**: p. 70-84.
101. Kim, J. and S. Hong, *A novel single-pass reverse osmosis configuration for high-purity water production and low energy consumption in seawater desalination.* Desalination, 2018. **429**: p. 142-154.
102. Voutchkov, N., *Energy use for membrane seawater desalination – current status and trends.* Desalination, 2018. **431**: p. 2-14.
103. Han, D., M. Hwang, and I.S. Kim, *Effect of boron rejection and recovery rate on a single-pass design of SWRO using hybrid membrane inter-stage design (HID) concept.* Desalination, 2017. **404**: p. 215-223.
104. Peñate, B. and L. García-Rodríguez, *Reverse osmosis hybrid membrane inter-stage design: A comparative performance assessment.* Desalination, 2011. **281**: p. 354-363.
105. Molina, V.G., M. Busch, and P. Sehn, *Cost savings by novel seawater reverse osmosis elements and design concepts.* Desalination and Water Treatment, 2009. **7**(1-3): p. 160-177.
106. Jeong, K., et al., *A systematic optimization of Internally Staged Design (ISD) for a full-scale reverse osmosis process.* Journal of Membrane Science, 2017. **540**: p. 285-296.
107. Park, M., et al., *Modeling of colloidal fouling in forward osmosis membrane: Effects of reverse draw solution permeation.* Desalination, 2013. **314**: p. 115-123.
108. Chen, K.L., et al., *The development of membrane fouling in full-scale RO processes.* Journal of Membrane Science, 2004. **232**(1): p. 63-72.
109. Kim, D.Y., et al., *Online estimation of fouling development for SWRO system using real data.* Desalination, 2009. **247**(1): p. 200-209.
110. Kim, M.J., B. Sankararao, and C.K. Yoo, *Determination of MBR fouling and chemical cleaning interval using statistical methods applied on dynamic index data.* Journal of

Membrane Science, 2011. **375**(1): p. 345-353.
111. Peiris, R.H., et al., *Fouling control and optimization of a drinking water membrane filtration process with real-time model parameter adaptation using fluorescence and permeate flux measurements.* Journal of Process Control, 2013. **23**(1): p. 70-77.
112. Kotb, H., E.H. Amer, and K.A. Ibrahim, *On the optimization of RO (Reverse Osmosis) system arrangements and their operating conditions.* Energy, 2016. **103**: p. 127-150.
113. Al-Obaidi, M.A., C. Kara-Zaïtri, and I.M. Mujtaba, *Simulation and optimisation of a two-stage/two-pass reverse osmosis system for improved removal of chlorophenol from wastewater.* Journal of Water Process Engineering, 2018. **22**: p. 131-137.
114. Rodriguez, S.G.S., *Particulate and Organic Matter Fouling of Seawater Reverse Osmosis Systems: Characterization, Modelling and Applications. UNESCO-IHE PhD Thesis*. 2011: CRC Press.
115. Tomaszewska, B., et al., *Use of numerical modelling in the prediction of membrane scaling. Reaction between antiscalants and feedwater.* Desalination, 2018. **427**: p. 27-34.
116. Khayet, M. and C. Cojocaru, *Artificial neural network modeling and optimization of desalination by air gap membrane distillation.* Separation and Purification Technology, 2012. **86**: p. 171-182.
117. Kleijnen, J.P., *Response surface methodology for constrained simulation optimization: An overview.* Simulation Modelling Practice and Theory, 2008. **16**(1): p. 50-64.
118. Sarkar, B., et al., *Prediction of permeate flux during electric field enhanced cross-flow ultrafiltration—a neural network approach.* Separation and purification technology, 2009. **65**(3): p. 260-268.
119. Labban, O., et al., *Fundamentals of low-pressure nanofiltration: Membrane characterization, modeling, and understanding the multi-ionic interactions in water softening.* Journal of Membrane Science, 2017. **521**: p. 18-32.
120. Wang, X.-L., et al., *Characterization and applications of nanofiltration membranes: State of the art.* Desalination, 2009. **236**(1): p. 316-326.
121. Wang, X.-L., et al., *Electrolyte transport through nanofiltration membranes by the space-charge model and the comparison with Teorell-Meyer-Sievers model.* Journal of Membrane Science, 1995. **103**(1): p. 117-133.
122. Waddell, L.S., *Chapter 205 - Colloid Osmotic Pressure And Osmolality*, in *Small Animal Critical Care Medicine*, D.C. Silverstein and K. Hopper, Editors. 2009, W.B. Saunders: Saint Louis. p. 868-871.
123. Vezzani, D. and S. Bandini, *Donnan equilibrium and dielectric exclusion for characterization of nanofiltration membranes.* Desalination, 2002. **149**(1): p. 477-483.
124. Kowalik-Klimczak, A., M. Zalewski, and P. Gierycz, *Removal of Cr(III) ions from salt solution by nanofiltration: experimental and modelling analysis.* 2016. **18**(3): p. 10.
125. Kong, F.-x., et al., *Assessment of the hindered transport model in predicting the rejection of trace organic compounds by nanofiltration.* Journal of Membrane Science, 2016. **498**: p. 57-66.
126. Abdellah, M.H., et al., *Organic solvent nanofiltration of binary vegetable oil/terpene mixtures: Experiments and modelling.* Journal of Membrane Science, 2019. **573**: p. 694-703.
127. Ochando-Pulido, J.M., M. Stoller, and A. Martinez-Ferez, *Boundary flux modelling for purification optimization of differently-pretreated agro-industrial wastewater with nanofiltration.* Separation and Purification Technology, 2018. **193**: p. 147-154.

128. Stoller, M., M. Bravi, and A. Chianese, *Threshold flux measurements of a nanofiltration membrane module by critical flux data conversion.* Desalination, 2013. **315**: p. 142-148.
129. Field, R.W., et al., *Critical flux concept for microfiltration fouling.* Journal of Membrane Science, 1995. **100**(3): p. 259-272.
130. Field, R.W. and G.K. Pearce, *Critical, sustainable and threshold fluxes for membrane filtration with water industry applications.* Advances in Colloid and Interface Science, 2011. **164**(1): p. 38-44.
131. Stoller, M. and J.M. Ochando-Pulido, *About merging threshold and critical flux concepts into a single one: the boundary flux.* The Scientific World Journal, 2014. **2014**.
132. Wang, X.-L., et al., *The electrostatic and steric-hindrance model for the transport of charged solutes through nanofiltration membranes.* Journal of Membrane Science, 1997. **135**(1): p. 19-32.
133. Kotyk, A., *Cell Membrane Transport: Principles and Techniques*. 2012: Springer US.
134. Silva, V., et al., *Alternative pore hindrance factors: What one should be used for nanofiltration modelization?* Desalination, 2009. **245**(1): p. 606-613.
135. Bungay, P.M. and H. Brenner, *The motion of a closely-fitting sphere in a fluid-filled tube.* International Journal of Multiphase Flow, 1973. **1**(1): p. 25-56.
136. Phuntsho, S., et al., *Osmotic equilibrium in the forward osmosis process: Modelling, experiments and implications for process performance.* Journal of Membrane Science, 2014. **453**: p. 240-252.
137. Xie, M., et al., *Relating rejection of trace organic contaminants to membrane properties in forward osmosis: Measurements, modelling and implications.* Water Research, 2014. **49**: p. 265-274.
138. Lee, J., et al., *A statistics-based forward osmosis membrane characterization method without pressurized reverse osmosis experiment.* Desalination, 2017. **403**: p. 36-45.
139. Attarde, D., M. Jain, and S.K. Gupta, *Modeling of a forward osmosis and a pressure-retarded osmosis spiral wound module using the Spiegler-Kedem model and experimental validation.* Separation and Purification Technology, 2016. **164**: p. 182-197.
140. Wang, Q., et al., *Modeling and measurement of temperature and draw solution concentration induced water flux increment efficiencies in the forward osmosis membrane process.* Desalination, 2019. **452**: p. 75-86.
141. Filippini, G., et al., *Performance analysis of hybrid system of multi effect distillation and reverse osmosis for seawater desalination via modelling and simulation.* Desalination, 2018. **448**: p. 21-35.
142. Chan, Y., *Mathematical Modelling on Seawater Desalination Using Nanomaterials.* Materials Today: Proceedings, 2015. **2**(1): p. 113-117.
143. Shahzad, M.W., M. Burhan, and K.C. Ng, *Pushing desalination recovery to the maximum limit: Membrane and thermal processes integration.* Desalination, 2017. **416**: p. 54-64.
144. Qasim, M., et al., *Reverse osmosis desalination: A state-of-the-art review.* Desalination, 2019. **459**: p. 59-104.
145. Budhiraja, P. and A.A. Fares, *Studies of scale formation and optimization of antiscalant dosing in multi-effect thermal desalination units.* Desalination, 2008. **220**(1): p. 313-325.
146. Singh, R., *Chapter 1 - Introduction to Membrane Technology*, in *Membrane Technology and Engineering for Water Purification (Second Edition)*, R. Singh, Editor. 2015, Butterworth-Heinemann: Oxford. p. 1-80.
147. Xie, M., et al., *Role of pressure in organic fouling in forward osmosis and reverse osmosis.*

Journal of Membrane Science, 2015. **493**: p. 748-754.
148. Altaee, A. and G. Zaragoza, *A conceptual design of low fouling and high recovery FO–MSF desalination plant.* Desalination, 2014. **343**: p. 2-7.
149. Altaee, A., A. Mabrouk, and K. Bourouni, *A novel Forward osmosis membrane pretreatment of seawater for thermal desalination processes.* Desalination, 2013. **326**: p. 19-29.
150. Altaee, A., et al., *Forward osmosis pretreatment of seawater to thermal desalination: High temperature FO-MSF/MED hybrid system.* Desalination, 2014. **339**: p. 18-25.
151. Pal, P., et al., *Modelling forward osmosis-nanofiltration integrated process for treatment and recirculation of leather industry wastewater.* Computers & Chemical Engineering, 2019. **127**: p. 99-110.
152. Mohammad, A.W., *A modified Donnan–steric-pore model for predicting flux and rejection of dye/NaCl mixture in nanofiltration membranes.* Separation Science and Technology, 2002. **37**(5): p. 1009-1029.
153. Zaviska, F. and L. Zou, *Using modelling approach to validate a bench scale forward osmosis pre-treatment process for desalination.* Desalination, 2014. **350**: p. 1-13.
154. S, S. and S. S, *Reverse Osmosis–Pressure Retarded Osmosis hybrid system: Modelling, simulation and optimization.* Desalination, 2016. **389**: p. 78-97.
155. Al-Obaidi, M.A., et al., *Performance analysis of a medium-sized industrial reverse osmosis brackish water desalination plant.* Desalination, 2018. **443**: p. 272-284.
156. Malik, S.N., P.A. Bahri, and L.T.T. Vu, *Steady state optimization of design and operation of desalination systems using Aspen Custom Modeler.* Computers & Chemical Engineering, 2016. **91**: p. 247-256.
157. Bartholomew, T.V., N.S. Siefert, and M.S. Mauter, *Cost optimization of osmotically assisted reverse osmosis.* Environmental science & technology, 2018. **52**(20): p. 11813-11821.
158. IRENA, *Renewable Energy Market Analysis: GCC*. 2019.
159. Al-Karaghouli, A. and L.L. Kazmerski, *Energy consumption and water production cost of conventional and renewable-energy-powered desalination processes.* Renewable and Sustainable Energy Reviews, 2013. **24**: p. 343-356.
160. Albloushi, A., et al., *Chapter 7 - Renewable Energy-Powered Membrane Systems for Water Desalination*, in *Current Trends and Future Developments on (Bio-) Membranes*, A. Basile, A. Cassano, and A. Figoli, Editors. 2019, Elsevier. p. 153-177.
161. Abdelkareem, M.A., et al., *Recent progress in the use of renewable energy sources to power water desalination plants.* Desalination, 2018. **435**: p. 97-113.
162. Ali, A., et al., *Membrane technology in renewable-energy-driven desalination.* Renewable and Sustainable Energy Reviews, 2018. **81**: p. 1-21.
163. Ghaffour, N., et al., *Renewable energy-driven innovative energy-efficient desalination technologies.* Applied Energy, 2014. **136**: p. 1155-1165.
164. Eltawil, M.A., Z. Zhengming, and L. Yuan, *A review of renewable energy technologies integrated with desalination systems.* Renewable and Sustainable Energy Reviews, 2009. **13**(9): p. 2245-2262.
165. Padrón, I., et al., *Assessment of Hybrid Renewable Energy Systems to supplied energy to Autonomous Desalination Systems in two islands of the Canary Archipelago.* Renewable and Sustainable Energy Reviews, 2019. **101**: p. 221-230.
166. Kershman, S.A., et al., *Hybrid wind/PV and conventional power for desalination in*

Libya—GECOL's facility for medium and small scale research at Ras Ejder. Desalination, 2005. **183**(1-3): p. 1-12.
167. Hossam-Eldin, A., A. El-Nashar, and A. Ismaiel, *Investigation into economical desalination using optimized hybrid renewable energy system.* International Journal of Electrical Power & Energy Systems, 2012. **43**(1): p. 1393-1400.
168. Khattab, N., et al., *Hybrid renewable energy system for water desalination: a case study for small green house hydroponic cultivation in Egypt.* ARPN journal of engineering and applies sciences, 2016. **11**(21).
169. Khan, M.A., S. Rehman, and F.A. Al-Sulaiman, *A hybrid renewable energy system as a potential energy source for water desalination using reverse osmosis: A review.* Renewable and Sustainable Energy Reviews, 2018. **97**: p. 456-477.
170. Pugsley, A., et al., *Global applicability of solar desalination.* Renewable Energy, 2016. **88**: p. 200-219.
171. Kasaeian, A., F. Rajaee, and W.-M. Yan, *Osmotic desalination by solar energy: A critical review.* Renewable Energy, 2019. **134**: p. 1473-1490.
172. Ahmed, F.E., R. Hashaikeh, and N. Hilal, *Solar powered desalination–Technology, energy and future outlook.* Desalination, 2019. **453**: p. 54-76.
173. Mentis, D., et al., *Desalination using renewable energy sources on the arid islands of South Aegean Sea.* Energy, 2016. **94**: p. 262-272.
174. Salehi, S., et al., *Multi-objective optimization of two double-flash geothermal power plants integrated with absorption heat transformation and water desalination.* Journal of Cleaner Production, 2018. **195**: p. 796-809.
175. Heidary, B., et al., *Optimal integration of small scale hybrid solar wind RO-MSF desalination system.* Renewable Energy Focus, 2018. **27**: p. 120-134.

6. Abbreviations

RO	reverse osmosis
MED	multi-effect distillation
MSF	multi-stage flash
MSF-BR	multi-stage flash brine recycle
MSF-OT	multi-stage flash once-through
MSF-M	multi-stage flash simple mixing
FO	forward osmosis
NF	nanofiltration
TBT	top brine temperature

ERD	energy recovery device
TDS	total dissolved solids
SSRO	single-stage reverse osmosis
SWRO	seawater reverse osmosis
BWRO	brackish water reverse osmosis
SEC	specific energy consumption
TrOC	trace organic contaminant
FMSI	FO pretreatment-MED Scale Index
RSI	Ryznar Scale Index
TCF	temperature correction factor
CPF	concentration polarization factor
CP	concentration polarization
SHP	steric-hindrance pore
TMS	Teorell-Meyer-Sievers
DE	differential evolution
ANN	artificial neural network
SK	Spiegler-Kedem model

7. Symbols

C_b	Bulk ion concentration
C_i	Ion concentration at solid-liquid interface
C_s	Saturation ion concentration
A_m	Water permeability coefficient
J_s	Salt flux

J_w	Pure water flux
ΔP	Transmembrane pressure difference
$\Delta \pi$	Osmotic pressure difference
B	Salt permeability coefficient
C_w	Salt concentration at membrane surface on the feed side
Cp	Permeate salt concentration
ε	membrane porosity
l	membrane thickness
r_p	pore radius
T_{hs}	heating steam temperature
M_r	recycled brine flow rate
M_{cw}	cooling water flowrate
M_f	Make-up seawater flow rate
R	membrane resistance
R_m	intrinsic membrane resistance
R_c	cake layer resistance
π_i	osmotic pressure of the active layer-support layer interface
π_a	osmotic pressure of the active layer surface
μ	dynamic viscosity
RR	recovery rate
α	dimensionless relative applied pressure
ε	dimensionless relative excess pressure ($\varepsilon = P_{ex} / \pi_o$)
P_{ex}	excess pressure

π_o	initial osmotic pressure
N	Number of stages
Φ	Final relative permeate volume
ΔP_{device}	applied pressure [bar]
$Q_{f,device}$	feed flow rate [m3/day]
η_{device}	efficiency
E_w	energy consumption $[kWh/d]$
$Q_{p,sys}$	total permeate produced from the RO system [m^3/d]
Q_p	permeate flow rate